Feasibility study of a vertical slit for the LBS line of the Linac4

Thesis to Attain the Degree of Master in Materials Science
CERN site de Prevessin. March-july 2012
Alexandre Ouzia

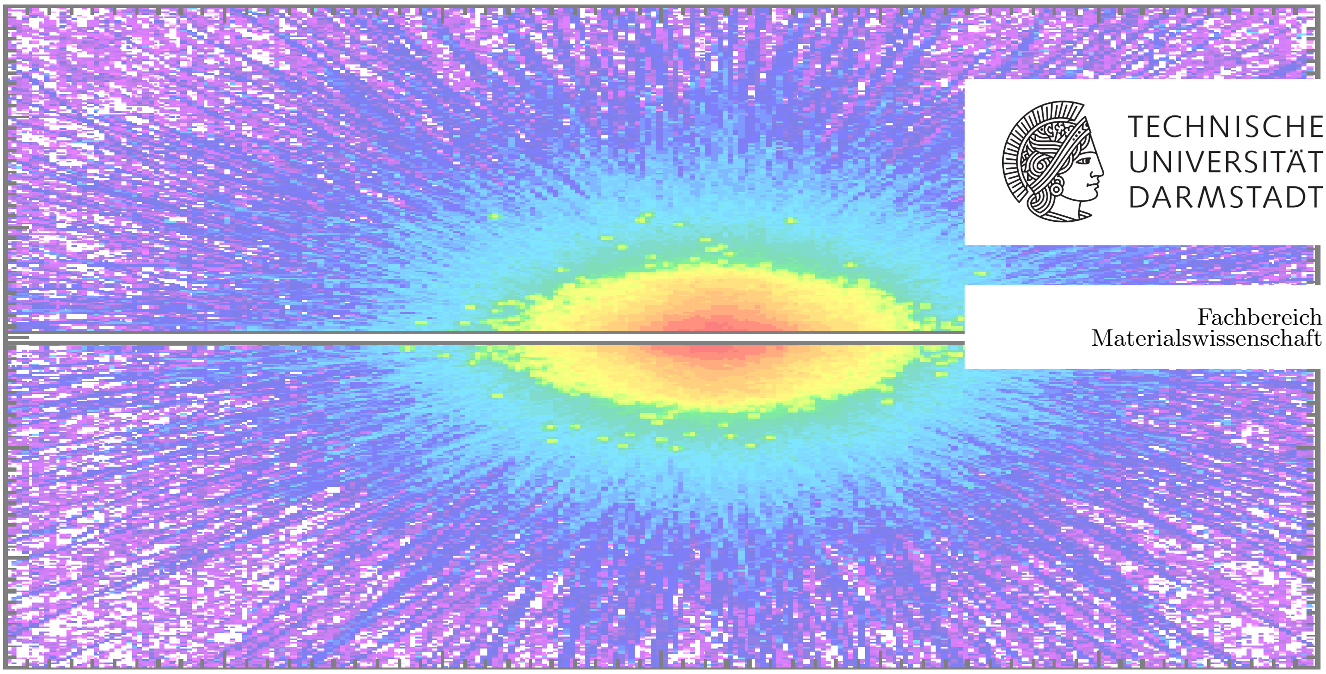

TECHNISCHE
UNIVERSITÄT
DARMSTADT

Fachbereich
Materialswissenschaft

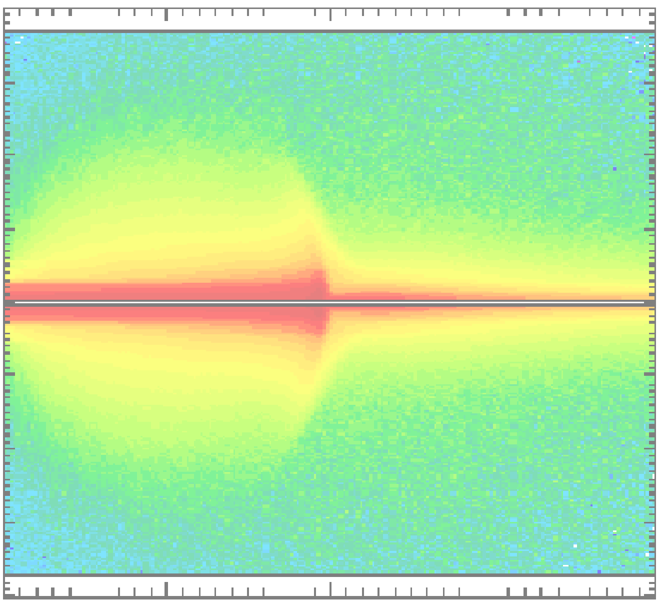

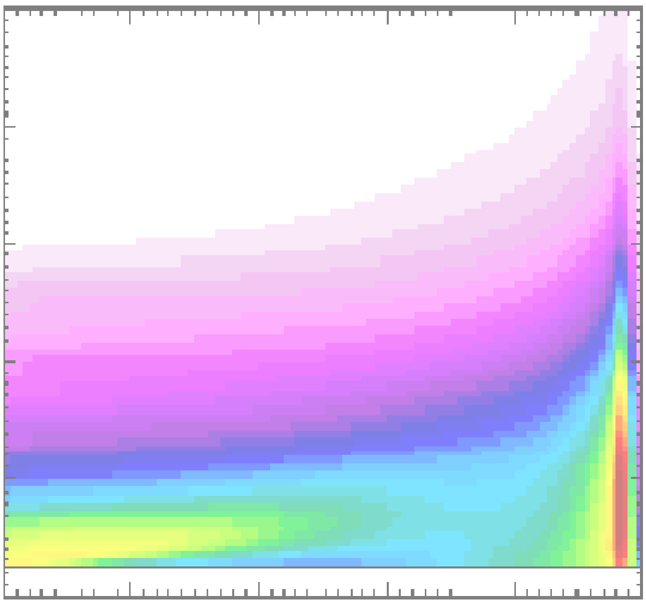

Feasibility study of a vertical slit for the LBS line of the Linac4
Thesis to Attain the Degree of Master in Materials Science
CERN site de Prevessin. March-july 2012

Submitted by Alexandre Ouzia
Date of submission: 7. September 2012

Supervisor: Dr. Habil. Adam Balogh

External Supervisor: I.Leitao and C.Maglioni

Technische Universitat Darmstadt
Fachbereich Materialswissenschaft

Prof. Dr. Habil. Adam Balogh

Abstract

The feasibility study of a vertical Slit was performed. This Slit is needed for the diagnostic Line for Beam energy Spread of the Linac 4 (LBS line). The Linac 4 will replace the Linac 2 and enable the Large Hadron Collider (LHC) to reach an energy of 14 TeV (highest energy ever reached).

When the beam impact on it, the Slit heats up and deforms. The deformation of the slit is the key problem. The present feasibility study aims at assessing whether or not it is feasible to keep this deformation below $50\mu m$, according to the specifications [14].

The determination of all the issues related with the Slit was driven. The priority was given to the thermomechanical issues. The methodology chosen to approach the problem led to three steps:

- First, the determination of possible designs for the Slit. One design was identified.
- Second, the determination of the best materials. Two figures of merit and a model were specifically conceived for it. Graphite R4550 was identified as the best material.
- Third, the Monte-Carlo FLUKA code and the numerical simulation software ANSYS were used to evaluate the deformation, temperature and stress state of the Slit.

The thesis concludes by stating that such a Slit is feasible and proposes a design.

Declaration of Originality

I herewith declare that I have produced this paper without the prohibited assistance of third parties and without making use of aids other than those specified; notions taken over directly or indirectly from other sources have been identified as such : the CERN website has been extensively used for the presentation of the CERN (section 1.2), and the book from M.Ashby [10] was particularly useful for the approach of the problem (section 3.4).

The master thesis was conducted from the 5 March 2012 to the 31 July 2012 under the supervision of I.Leitao and C.Maglioni at CERN on the prevesin site in the EN-STI-TCD section.

Geneva, the 7. September 2012 Alexandre Ouzia

Acknowlegments

I would like to thank several people who help me over the last five months. First I would like to thank my two supervisors at CERN, Ivo and Cesare for the opportunity they gave to work in such a nice environment and directions they gave during my thesis. I am also especially grateful toward Prof.Balogh and Marilena Tomut, my last supervisor when I was at GSI, who provided me insights about the materials behaviour under irradiation.

I also really appreciated the daily life at CERN in the TCD team. I therefore would like to thank all my team members. Finally and maybe most importantly I am grateful to Melanie and Tryphon for all the passionate discussions (and sometimes passionate disagreements ...) about radiative cooling or waves propagations in various media we had together.

Contents

List of Figures

List of Tables

1 Introduction and Perspective

1.1 How far the present study is integrated in the CERN project

Before reaching the Large Hadron Collider (LHC), particles are produced at the sources and accelerated by a set of preaccelerators: linear accelerators and synchrotrons. The Linac 4 is a linear accelerator which will replace the Linac 2 as injector to the Proton Synchrotron Booster (PSB [1]).

The goal of the Linac 4 project is to build a 160 MeV H linear accelerator replacing Linac 2 as injector to the PS Booster (PSB). The new linac is expected to increase the beam brightness out of the PSB by a factor of 2, making possible an upgrade of the LHC injectors for higher intensity and eventually an increase of the LHC luminosity [1].

Before the beam escapes the Linac 4 to reach the PSB, the energy spread of the beam is checked along the the Line for Beam energy Spread (LBS line). The present thesis focuses on the feasibility study of a vertical slit which will be used in the LBS line.

1.2 CERN highlights

CERN stands for "Centre Europeen de Recherche Nucleaire": european center for nuclear research.

The range and number of experiments currently running at CERN is too wide to be presented in a few pages. What follows only gives highlights of a few major aspects. For more details, links to relevant pages are proposed. The acronym are defined in the glossary.

Most of what follows is directly selected from the CERN presentation website: `http://public.web.cern.ch/public/en/About/About-en.html`.

1.2.1 The CERN accelerator facility

The CERN accelerator facility is a succession of particle accelerators that can reach increasingly higher energies (see figure 1.1). Each accelerator boosts the speed of a beam of particles, before injecting it into the next one in the sequence.

The facility also includes the Antiproton Decelerator and the ISOLDE facility and feeds the CNGS project and the CLIC test area (CTF3).

FOUNDATION: 1954
PLACE: Geneva
ASSOCIATES: 20 member states
BUDGET: 1 billion € a year
STAFF: 20000 employees
NOBEL PRIZES: 6

Protons are obtained by removing electrons from hydrogen atoms. They are injected from the linear accelerator (Linac 2) into the PS Booster, then the Proton Synchrotron (PS), followed by the Super Proton Synchrotron (SPS), before finally reaching the Large Hadron Collider (LHC). Protons will circulate in the LHC for 20 minutes before reaching the maximum speed and energy.

Lead ions for the LHC start from a source of vaporised lead and enter Linac3 before being collected and accelerated in the Low Energy Ion Ring (LEIR). They then follow the same route to maximum acceleration as the protons.

1.2.2 CERN experiments

Physicists at CERN perform a wide range of experiments, which use beams of energetic particles produced in the accelerator facility. Each experiment involves specialised equipment, the detectors, to record what happens when the beam hits either a fixed target or particles in a similar beam coming from the opposite direction.

At the lowest energies, the Proton-Synchrotron Booster supplies beam to ISOLDE, a unique source of radioactive isotopes for experiments with applications that range from astrophysics to industry and medicine.

The Proton Synchrotron (PS) delivers higher energy protons to two contrasting experiments. DIRAC is testing ideas about the strong fundamental force, while CLOUD is finding out how natural high-energy particles might influence the formation of clouds. The PS also provides the protons that create the antiprotons for the Antiproton Decelerator (AD), where physicists are learning more about antimatter in the ALPHA, ASACUSA and ATRAP experiments. The ACE experiment also uses antiprotons, in this case to assess their suitability for cancer therapy.

The next largest accelerator is the Super Proton Synchrotron (SPS), where COMPASS focuses on investigating hadrons - particles made of quarks, including the nucleons (protons and neutrons) of ordinary matter.

The Large Hadron Collider (LHC), CERNs most powerful accelerator, hosts six experiments designed to find out how the particles of matter behave at a new high energy frontier. The experiments are located at points where the LHCs two beams, which travel in opposite directions, collide head on.

For more information about the LHC experiments: `http://public.web.cern.ch/public/en/LHC/LHCExperiments-en.html`. For more information on non-LHC experiments: `http://public.web.cern.ch/public/en/Research/OtherExp-en.html`.

1.2.3 The Higgs Boson

The existence of new boson around 126 GeV was announced at the CERN semi-annual conference on the 4th of July. Its behaviour is said to be consistent with the predicted Higgs boson. The discovery of the Higgs boson was one of the main reason for the construction of the LHC. It is however not the end of the story as Rolf Heuer, the president of the CERN, said [1], but the beginning. Other questions are raised, such as:

- What are the properties of that particle ?
- Are there any other Higgs bosons or is it the only one ?

[1] I was personnaly there and heared him

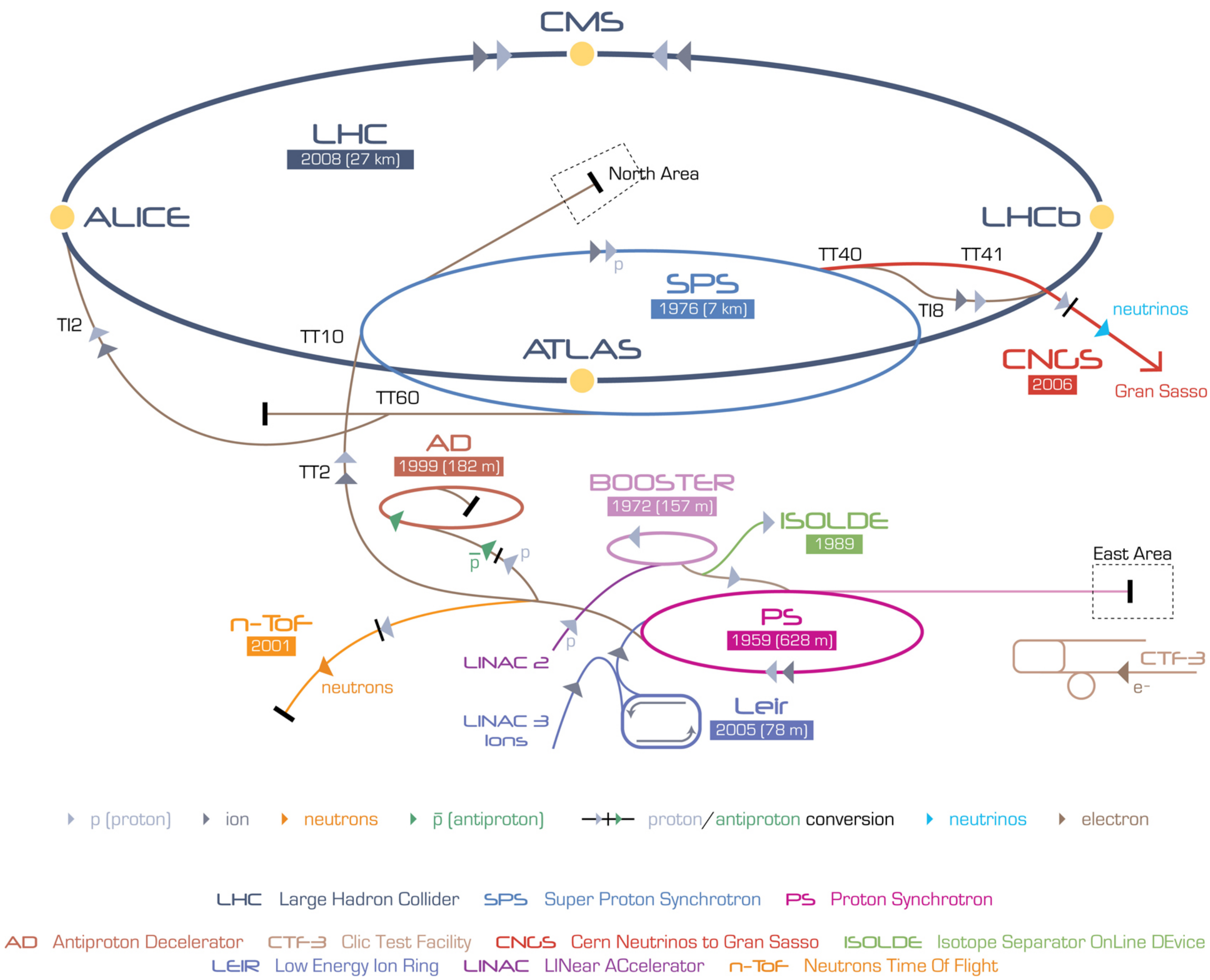

Figure 1.1.: The CERN accelerator facility [?]. Each experiment and accelerator has a dedicated website.

2 Motivations

In order to assess the quality of the beam at the exit of the Linac 4, two diagnostic lines exist: the Line for Beam Emittance measurement (LBE) and the Line for Beam energy Spread measurement (LBS). The quantity describing the energy spread is $\frac{dp}{p}$. The measurement principle of the LBS line requires the installation of a vertical slit (abstract of [8]). This is the motivation.

The central element of this diagnostic line is a vertical spectrometer magnet, which sorts the particles according to their individual energy along a vertical position axis. From the central value of this distribution the mean energy can be derived, while the width of the distribution is proportional to the beam energy spread (abstract of [8]). The layout is presented on figure 2.1.

The following formula connects $\frac{dp}{p}$ to the measured beam radius:

$$\frac{dp}{p} = \frac{1}{D}\sqrt{\sigma_{measured}^2 - (\epsilon\beta)^2} \tag{2.1}$$

where:

- D is the dispersion (known)
- $\frac{dp}{p}$ is the relative momentum spread
- β is the usual beta function
- ϵ is the emittance of the beam
- $\sigma_{measured}$ is the half-width of the gaussian distribution of the beam spread

The relative momentum spread can only be calculated if the $\epsilon\beta$ term is small compared to $\sigma_{measured}$. The slit intervenes precisely in reducing the emittance (ϵ), and the measurement instrument (SEM grid) is placed at the minimum of the β function, so that:

$$\frac{dp}{p} \simeq \frac{1}{D}\sigma_{measured} \tag{2.2}$$

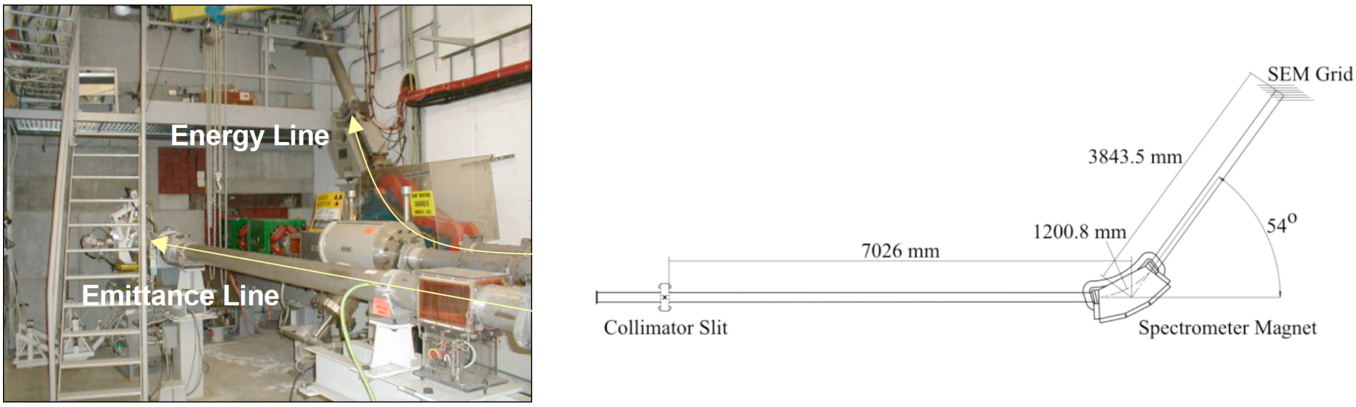

Figure 2.1.: On the left: Photograph of the present installation of the two diagnostic lines. On the right: schematic layout of the present energy measurement line. The distances and the bending angle read as they are implemented for Linac2 [15]

3 Formulation of the Problem

3.1 First Formulation

The purpose of the Slit is to vertically cut the beam. Figure 3.1 represents a sketch of a typical Slit. In order to fulfil its function, the aperture of the Slit must remain constant during operation. To put it another way, the surfaces of the aperture of the Slit must not deform too much [1].

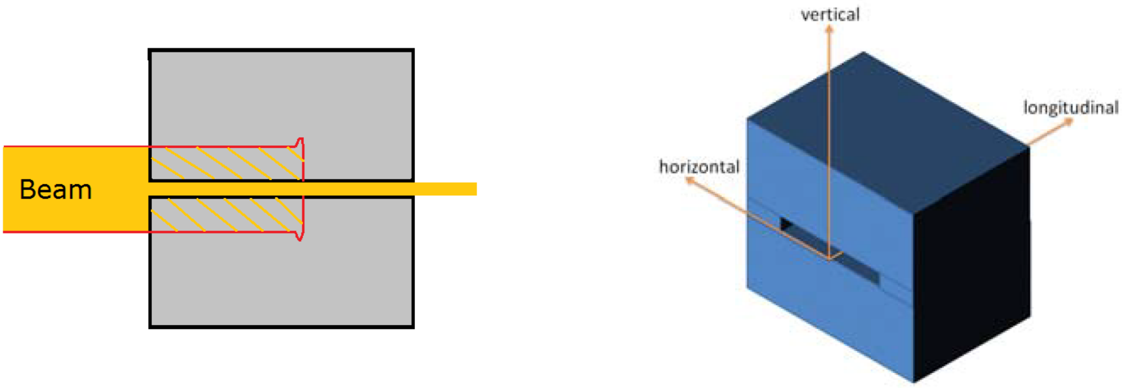

(a) Sketch of a typical Slit in 2D.

(b) Sketch of a typical Slit in 3D.

Figure 3.1.: One part of the beam goes through the aperture while the other one impacts on it and stops. The part that impacts on the Slit heats it. The Slit, being heated, dilates: it deforms. In order to fulfil its function, the aperture of the Slit must not deform too much.

However upon irradiation by 160 MeV protons, the Slit heats up and does deform. In first approach, the problem can be formulated:

> "How to keep the deformation of the Slit as low as possible ?"

On what parameters does the deformation of the Slit depends ? First on the loading condition, i.e. the beam parameters, and second on the design of the Slit.

The beam parameters (power, energy of the particles and spatial distribution) are fixed by the specifications [14] (Appendix A). The only free variable is the design, i.e. the material and the geometry.

The choice of the material impacts on the deformation because some materials may heat and deform more than others. Similarly the geometry, especially the shape of the impacted area impacts on how the heat is spread on the surface and in the volume[2].

Since the only free variables of the problem are the geometry and the material, a second formulation of the problem would be:

> "What is the geometry and the material that minimize the aperture deformation" ?

[1] See the specifications in appendix A for the numerical values.

[2] See table 4.1 for the different shapes of the impacted area.

3.2 List of all issues

Although minimizing the aperture deformation is the key issue, it is not the only one.

Being a BID (Beam Intercepting Device), a Slit shares all the issues of BID. The BID themselves are a subclass of the engineering devices and thus share their issues: typically cost and maintenance. All these issues are summarized on figure 3.2.

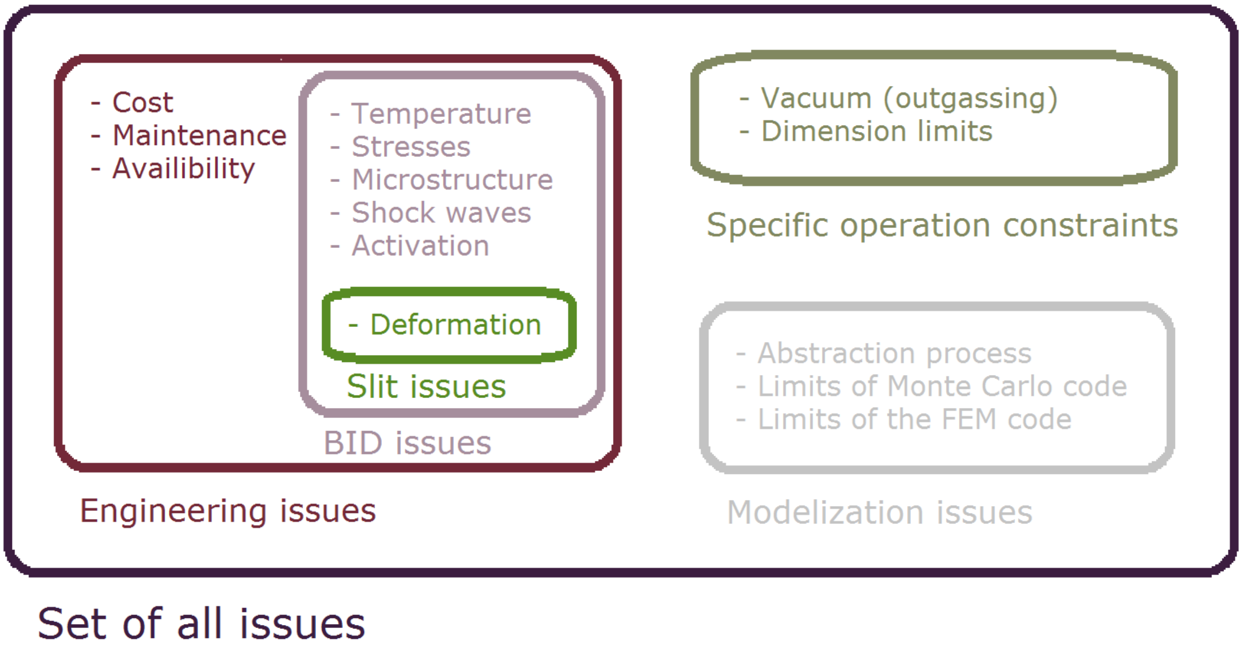

Figure 3.2.: Classification of all the issues. See the glossary for the abstraction process, the Monte-Carlo code and FEM.

Upon irradiation by 160 MeV, the Slit heats up and deforms, therefore stresses occur. The stress should be kept below the fatigue limit of the material[3]. Moreover, when the beam hit the Slit, a shock wave is produced. That might break it.

The microstructure of the material after irradiation should also be assessed, since the macroscopic thermomechanical properties of the Slit depend on it. Will the thermomechanical properties of the Slit be the same after a few weeks, months or years ?. The activation of the whole Slit should also be checked for radioprotection reasons.

Though less critical, vacuum aspects (the Slit is in vacuum) and dimension limits have to be taken into account.

Like all engineering instruments, the cost, maintenance and availability should be considered.

Finally, the problem will not be solved analytically but numerically using ANSYS workbench. The model depends on the quality of the abstraction process, the precision of the Monte-Carlo code (FLUKA) and the quality of the Finite-Element modelization (FEM) done with ANSYS.

3.3 Scope of the feasibility study

Now that all the issues have been enumerated, the problem can be exactly stated:

3 It might be first thought that the yield strength is the relevant criteria, but it is not. The beam being composed of pulses, it is discontinuous meaning that the stresses in the Slit are also cyclic.

> ”What is the optimal design and optimal material that suit all the issues?”

Yet, the present feasibility study does not deal exhaustively with all the issues. It focuses particularly on the Slit specific issues and those issues common with the BID. The thermomechanical issues are exhaustively treated (temperature,stresses and deformation). The other issues are only briefly discussed, but the keys to treat them are given.

Moreover the present feasibility does not provide the complete design of the Slit. The integration with the other parts of the beam line is not discussed at all. It only focuses on the design of the volume which interacts directly with the beam. In order to avoid any confusion, we introduce the word “predesign” to denote that part that interacts directly with the beam.

The present feasibility study answers with a systematic approach to the problematic:

> ”What predesign and what material best suit the temperature, stresses and deformation issues ?”

Then the predesign and the material selected are found to meet all the other issues (see the conclusion section).

3.4 Approach of the Problem

The methodology used to select the best predesign and material is based on the following assumption:

1. “Separation of predesign and material selection[4]”: the material choice is dependent of the predesign. The possible predesigns should be defined first, and only then figures of merit and materials selection for each predesign can be derived.
2. “predesign selection by literature review and imagination”: from literature review only a few designs are found. Two are presented.
3. “Selection of materials by figures of merit”: since there is no single currency to classify all the materials figures of merit are defined in order to eliminate materials that are likely not to be good candidates[5]. Then it appears that only a few materials are left.
4. “Finite element as the concluding step”: once a predesign and a material are identified as relevant candidates, three simulations are run to assess the temperature, stresses and deformation of the Slit. From theses three simulations the conclusion on the feasibility (or non feasibility) follows immediately.

[4] In general predesign and material selection interact. In general there exists for a predesign D_1 a best material M_1 and for another predesign D_2 a best material M_2 such that $M_1 \neq M_2$ (see section 7.6 on the selection of material and shape first paragraph of [10]).

[5] The conception of the figures of merit is done in the next chapter.

4 Predesign selection

There does not seem to exist a general and rigorous method to conceive the best predesign. Therefore the first step in the predesign selection was to browse through the literature and imagine new predesigns from it.

The predesign of a slit can be divided in five independent features[1]:

- the phase of the material
- the shape of the impacted area
- the cooling system
- the mechanical movement during operation
- the working temperature

The various possibilities are presented in table 4.1. By combining them, possible predesigns can be derived.

Some predesigns are simpler to build and to work with than others. For example a solid static block of copper with drilled water pipes would be much simpler than two rotating copper cylinders rotating in opposite directions and cooled down by water. However the latter predesign may have advantage the first has not (lower temperature and stresses levels for example).

The methodology chosen was to focus first on simple predesigns and check if they fail or not. If yes, more complex predesigns would then be analysed.

Among the various predesigns which were thought up, only two are presented.

4.1 predesign 1

The design 1 is composed of two symmetrical blocks and is presented on figure 4.1. Depending if the material is a metal or a ceramic, the cooling can be either convective (water flowing through pipes) or conductive[2] (using a copper jacket).

Refering to table 4.1, the beam impacts on a perpendicular area, there is no mechanical movement, the phase is solid and the working temperature low.

The main advantage of the design is its simplicity.

4.2 Predesign 2

The main difference with the predesign is the working temperature which is high. The cooling mode is radiative. The beam impacts on a block, and heats it. The block heats until it radiates as much energy as it receives. Around this block is another part which capture the emitted radiations. Since the temperature reached is high, high-temperature alloys and ceramics are of special choice.

The motivation to work at high temperature is twofold: first the specific heat capacity of most materials, especially the ceramics, increase significantly with temperature (see figure 4.3). When the heat capacity increases, the temperature gradient and therefore the stresses in the materials following the pulses decreases. Second, working at high temperature enables defects annealing.

[1] As far as we have found and imagined. Other features may also exist. The features chosen and presented in table 4.1 are not always independent: it is difficult to have a solid rotating slit cooled down by convection (water).

[2] Ceramics usually cannot be drilled.

Table 4.1: The five dimensions of a predesign are presented in the first column. By picking up one of the possibilities in each dimension, a predesign is found. For example: a shape of the impacted area with an angle cooled by convection (by drilling pipes), static, solid and working at high temperature. Other combinations are possible, but some of them may not be practical.

Shape of the impacted area	perpendicular 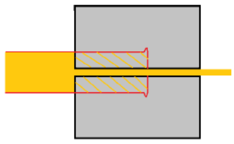	with an angle 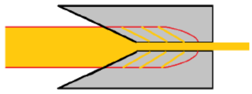	
cooling mode	conduction (jacket)	convection (drilled pipes)	radiation
mechanical movement	static	translating (⊥ to beam direction)	rotating 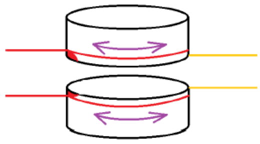
phase	liquid	solid	
working temperature	low	high	

4.3 Comparison of the two predesigns

The first design aims at simplicity, while the second aims at diminishing the stresses in the material. Predesign 2 is only interesting if the first one fails.

However, simulations were made, and the predesign 2 proved to be much more technologically challenging than the first one. Moreover though the stresses due to the pulses are indeed two times lower than with the predesign 1, others stresses appear. Indeed at the temperature reached the thermal conductivity of graphite decreased by nearly an order of magnitude, leading to a significant temperature gradient. Since the predesign 1 already proved feasible, no more research was done to solve the eventual issues of predesign 2.

The predesign 2 proves that the stresses due to the pulses are significantly reduced, but that other issues do appear.

4.4 Dimensions of the predesign

The range of 160 MeV protons in any material can be evaluated by SRIM and is shown in figure 4.4. The minimal depth is therefore of 14cm. Then depending on the material the depth may be reduced.

The width and height of the half-blocks of both designs should be large enough to capture 7σ of the

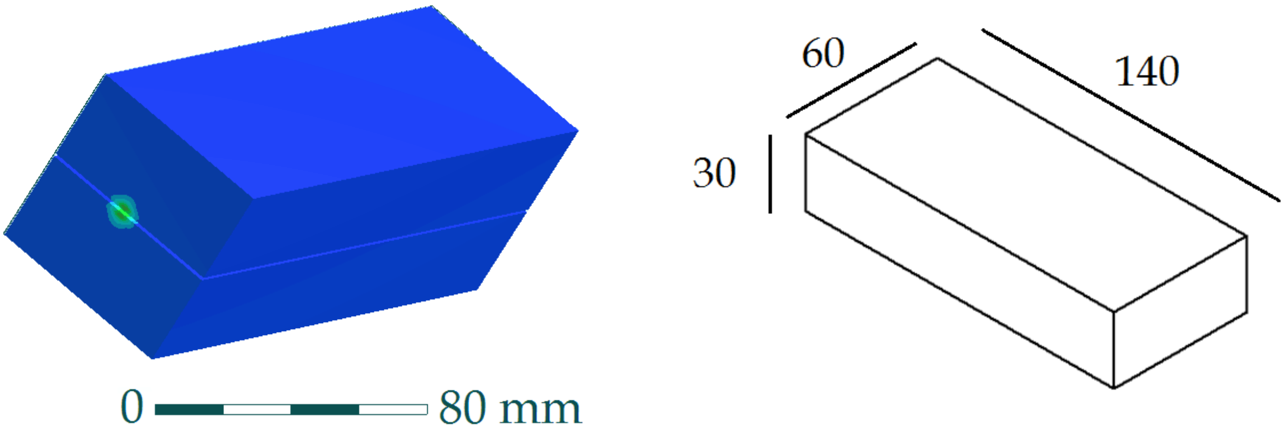

Figure 4.1.: Illustrations of the predesign 1. It reduces to two symmetrical blocks with an aperture of 1mm in between. On the left, the impact of the beam is represented in green, on the right the minimal dimensions of one of the two blocks are given in mm. Left figure made with ANSYS [13].

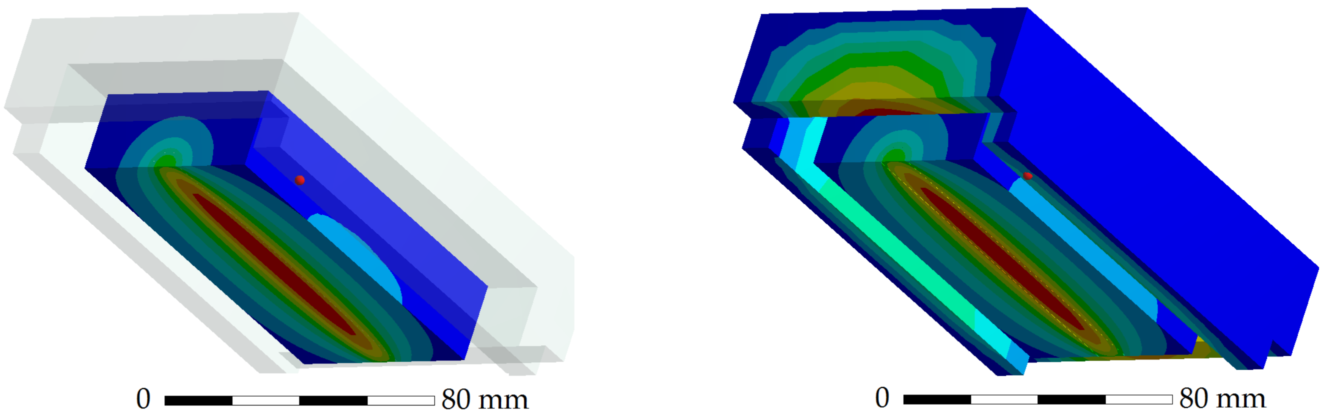

Figure 4.2.: Illustrations of the predesign 2. The beam impacts on the block shown on the left. This block heats to a temperature until the equilibrium with radiated energy is reached. The radiations are catched by the other part which is cooled by drilled pipes. The colors represents roughly where the hot (in red) and cold part would be. Figures made with ANSYS [13].

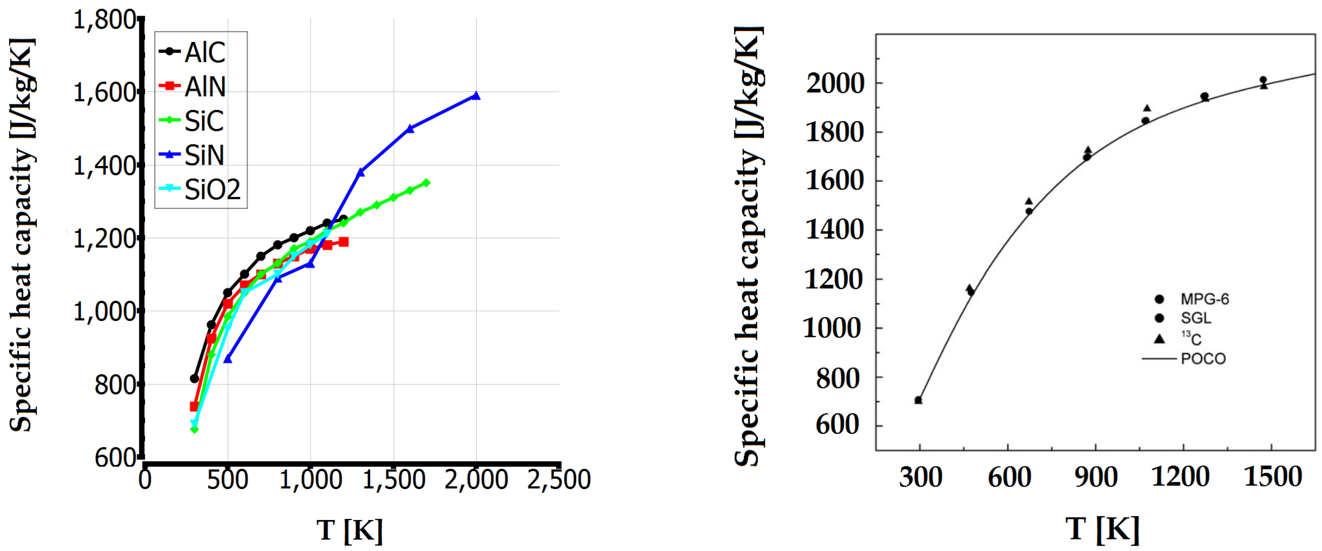

Figure 4.3.: Evolution of the specific heat capacity with temperature for a some ceramics (left) [9] and nuclear grades graphites (right) [6]. When the heat capacity increases, the temperature gradient and therefore the stresses in the materials following the pulses decreases. For graphite, for example, the specific heat capacity triples from room temperature to 1500K, which means the stresses would be divided by three by working at that temperature.

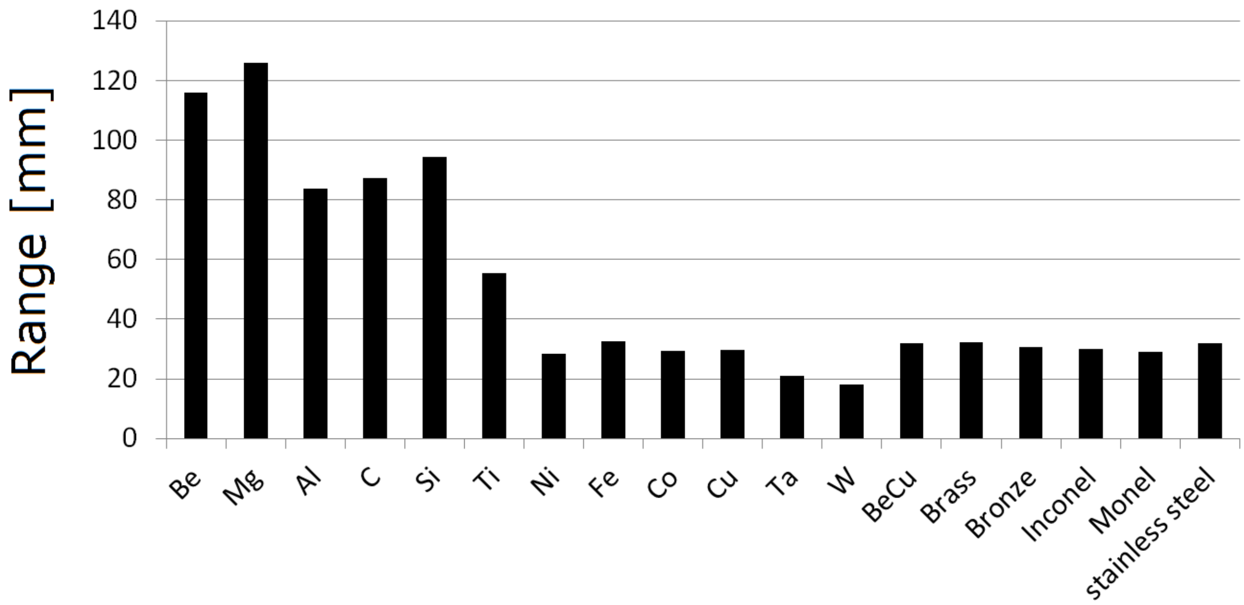

Figure 4.4.: Range of 160 MeV protons in common materials. These estimations are based on SRIM [7] calculations. Depending on the material, the slit should be between 20 and 140 mm to be safe.

beam, i.e $7 * 3mm = 2.1cm$ [3] for the height and twice for the width (symmetry). Figure 4.1 sums up minimal dimensions for the slit.

[3] The beam width is about 3mm. For more details see the datasheet in the appendix C.

5 Material selection

As explained in the approach (section 3.4), the materials are classified by figures of merit (FOM) that are first defined. Two thermomechanical FOMs are defined (section 5.1) and charts are used to select the candidate materials. A model has been specially built for these two figures of merit and is presented in appendix B. In our case, the set of candidates is reduced to only graphites and carbons.

5.1 Figures of Merit

Figures of merit[1] (FOMs) are:

> "the key to optimal material selection. For most load bearing components, performance is limited not to one but a combination of materials properties. Indices of performance are combination of material properties which, when maximised, maximise some aspect of the performance [10]."

Relevant comparison of material properties and loading conditions have therefore to be formulated and transformed into equations. In the present case (beam heating matter), the loading condition depends on the power of the beam and the properties of the material. Therefore correlations are needed to make the FOMs only rely on the properties of the material.

Once FOMs are produced, softwares such as CES[2] can draw charts to classify all the materials according to these FOMs. Such softwares possess a database of thousands of materials (3836 with the license used for the thesis) and all the usual mechanical and thermal properties of the materials.

To derive them, we propose the following "algorithm":

1. State in words the condition
2. Translate it into equation
3. Try to link the parameters to the intrinsic properties of the materials from their definition
4. If necessary, build a model linking the loading conditions to the intrinsic properties of the material
5. Rewrite the whole figure of merit

Temperature figure of merit

- statement: the maximal temperature in the material must remain below the maximal working temperature
- translation into equation: $T_{max} < T_{working}$
- link to intrinsic properties: $T_{max} = T_0 + T_{steadyState} + \Delta T pulse$
- use of a model[3]: $T_0 \simeq 300K$,$T_{SteadyState}$ would need a model (not developed). As an order of magnitude we take $100°$, which is the order of magnitude of the value found for graphite. $\Delta T_{pulse} \simeq \frac{3.10^6}{\rho^{0.186} C_p}$[4]
- final expression: $\frac{T_{max}}{T_{working}} = \frac{300+100+\Delta T_{Pulse}}{T_{working}}$

[1] or indices of performance.
[2] See glossary for information about it.
[3] The full description of the model used to evaluate ΔT_{pulse} is given in appendix B.
[4] idem.

Stress figure of merit

- statement: the maximal stress in the material must remain below the fatigue limit
- translation into equation: $\sigma_{max} < \sigma_{fatigue}$
- link to intrinsic properties: $\sigma_{max} = E\epsilon_{max} = E\alpha\Delta T_{pulse}$
- use of a model[5]: $\Delta T_{pulse} \simeq \frac{3.10^6}{\rho^{0.186} C_p}$[6].
- final expression: $\sigma' = \frac{\sigma_{max}}{\sigma_{fatigue}} = \frac{E\alpha}{\sigma_{fatigue}(1-2\nu)} \cdot \Delta T_{Pulse}$

5.2 Development of a model for ΔT_{pulse}

The stress figure of merit, as defined above, need the estimation of the maximal increase of temperature ΔT_{pulse} following a pulse. The model is presented in full details in appendix B.

Without going in all the details, we comment here its main results.

In the present case, the maximum increase of temperature occurs at the Bragg peak[7], and is given by:

$$\boxed{\Delta T_{Pulse}^{Bragg} = \frac{1}{\rho^{0.186} c_p} \cdot \frac{1.92.10^{-12} \cdot N_{particules}}{2\pi \cdot \sigma_{eq_x} \cdot \sigma_{eq_y}}} \tag{5.1}$$

where:

- ρ is the density of the material
- c_p the specific heat capacity
- $N_{particles}$ the number of particles in one beam pulse (no unit)
- σ_{eq_x} and σ_{eq_y} are the beam gaussian distribution widths in x and y directions

and

- $\sigma_{eq_x}^2 = \sigma_x^2 + \sigma_s^2$
- $\sigma_{eq_y}^2 = \sigma_y^2 + \sigma_s^2$

where σ_s is the average width of the beam gaussian distribution of one particle (the "s" is for straggling and scattering).
In its fully developped form, equation 5.1 is:

$$\boxed{\Delta T_{Pulse}^{Bragg} = \frac{1}{\rho^{0.186} c_p} \cdot \frac{1.92.10^{-12} \cdot N_{particules}}{2\pi \cdot \sqrt{\sigma_x^2 + \left(.25 \cdot \frac{Z^{\frac{1}{2.2}}}{\rho \cdot 73}\right)^2} \cdot \sqrt{\sigma_y^2 + \left(.25 \cdot \frac{Z^{\frac{1}{2.2}}}{\rho \cdot 73}\right)^2}}} \tag{5.2}$$

From this equation conclusions can be made:

- since the denominator of equation 5.1 is in the order of magnitude of 1, ΔT will be in the order of the magnitude of a few Kelvins if the numerator is also of the order of magnitude of 1, i.e. if $N_{particles} * 1.95.10^{-12} \simeq 1$ i.e. $N_{particles} \simeq 5.10^{11}$. This gives an order of magnitude of the number of particles in one pulse from which the temperature "really" increases.

5 The full description of the model used to evaluate ΔT_{pulse} is given in appendix B.
6 proved in section 5.3.
7 See glossary for Bragg peak.

- the importance of the density of the material relatively to the maximal increase of temperature is small since its exponent is small. It is interesting to notice that the only property of the material relevant here is the specific heat capacity.

5.3 CES Maps

The figures of merit which have been used to draw the CES [5] [8] charts are the following one:

$$\sigma^* = \frac{E\alpha\Delta T_{pulse}}{\sigma_{fatigue}\cdot(1-2\nu)} < 1 \tag{5.3}$$

$$T^* = \frac{400+\Delta T_{pulse}}{Twork} < 1 \tag{5.4}$$

By injecting the beam specifications in equation 5.2, we have:

$$\Delta T^{Bragg}_{Pulse} = \frac{1}{\rho^{0.186}c_p}\cdot\frac{1.92.10^{-12}\cdot N_{particules}}{2\pi\cdot\sigma_{eq_x}\cdot\sigma_{eq_y}}$$

$$= \frac{1}{\rho^{0.186}c_p}\cdot\frac{1.92.10^{-12}\cdot 9.96.10^{13}}{2\pi\cdot\sqrt{(2.2.10^{-3})^2+\left(.25\cdot\frac{Z^{\frac{1}{2.2}}}{\rho\cdot 73}\right)^2}\cdot\sqrt{(2.8.10^{-3})^2+\left(.25\cdot\frac{Z^{\frac{1}{2.2}}}{\rho\cdot 73}\right)^2}}$$

This equation can not however be taken as input directly in CES since the atomic mass Z of each material is not available in the datasheets of the CES database. Therefore, the term $\sigma_s = \left(.25\cdot\frac{Z^{\frac{1}{2.2}}}{\rho\cdot 73}\right)^2$ has been evaluated to 2mm, which is the average value for this energy[9].

With this approximation the equation becomes:

$$\Delta T^{Bragg}_{Pulse} = \frac{1}{\rho^{0.186}c_p}\cdot\frac{1.92.10^{-12}\cdot N_{particules}}{2\pi\cdot\sigma_{eq_x}\cdot\sigma_{eq_y}}$$

$$= \frac{1}{\rho^{0.186}c_p}\cdot\frac{1.92.10^{-12}\cdot 9.96.10^{13}}{2\pi\cdot\sqrt{(2.2.10^{-3})^2+(2.0.10^{-3})^2}\cdot\sqrt{(2.8.10^{-3})^2+(2.0.10^{-3})^2}}$$

$$= \frac{1}{\rho^{0.186}c_p}\cdot 2.97.10^6$$

$$\Delta T_{Bragg} \simeq \frac{3.10^6}{\rho^{0.186}c_p}$$

The equations used for the selection of materials in CES were therefore:

$$\sigma^* = \frac{E\alpha\frac{3.10^6}{\rho^{0.186}c_p}}{\sigma_{fatigue}\cdot(1-2\nu)} < 1 \tag{5.5}$$

$$T^* = \frac{400+\frac{3.10^6}{\rho^{0.186}c_p}}{Twork} < 1 \tag{5.6}$$

[8] CES [5] is a software. See the glossary for more details.
[9] This can be easily seen by lunching simulations with SRIM on usual materials.

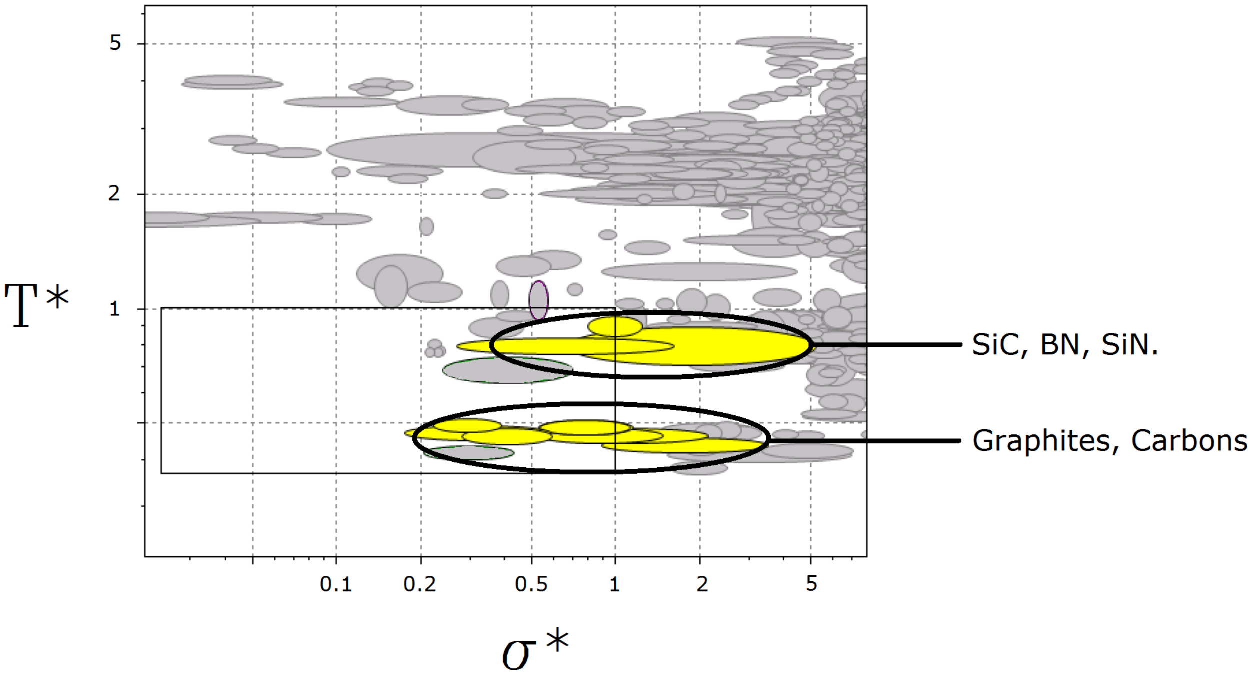

Figure 5.1.: Evolution of the temperature figure of merit with the sigma figure of merit [10]. Each material is represented by an ellipse. The grey materials are those who do not pass the conditions. The condition for acceptance is to be below one for both of the FOMs. Only a few materials are left (14 on 3836): in yellow are some graphites, carbons and other ceramics. Since graphites and carbons are closer to 0, they are the best candidates. The materials which appear in grey and are in the square either are not available as bulk materials (wires of filaments) or does not fit vacuum conditions (foams)). Chart made with CES [5].

5.4 Conclusion on the materials selected

From figure 5.1, the only candidate materials are graphites[11] and carbons. The already available graphite for BID at CERN is the R4550 graphite (see its datasheet in appendix C).

To be perfectly rigorous, the other issues (enumerated in table 4.1) should have been taken into account in the material selection. Two reasons led us not to consider them yet. First, most of them are not quantifiable (as for example the microstructure evolution). There is an practical impossibility to consider them. Second, the materials selected in the end (R4550 graphite) has already been tested and used at CERN for similar experiments, i.e. with similar issues. Moreover it is common knowledge that graphite is used in high-irradiation environment.

Now that we have only one possible class of materials and one predesign, three simulations are needed to conclude on the feasibility of the slit.

[11] idem.

6 Other issues

The thermomechanical evolution of the slit is the most important parameter in the deformation of the slit. This is however not the only one. Other issues should be taken into account to complete the feasibility study.

6.1 Microstructure evolution

Upon irradiation by energetic particles, radiation damages occurs. Common one are:

- ion track formation
- vacancies and voids creation
- defect formation: points, clusters, dislocations, protusions
- surface effects

The microstructure evolution necessary impacts on the macroscopic properties, especially on the mechanical and thermal properties.

The evolution of the mechanical and thermal properties eventually impacts on how the slit deforms.

To minimize the microstructure evolution, and thus remove one of the reason of deformation, the choice has been made to select amorphous materials. This is the case if the graphite is selected.

6.2 Charge accumulation

The incoming particles will necessary charge the slit when impacting on it. Moreover, during the impact on the incident surface, electrons may be ejected leading to an overall non-neutral slit. To avoid these two problems, a suppression grid (electrode with a cylindrical hole)can be placed 1cm before the incident surface. By applying a voltage between the slit and the grid, the electrons will be reflected back on the slit, and the surplus of electrons could be released through an external circuit.

6.3 Particles accumulation

When the beam impacts on the slit, the hydrogen particles stay inside at given depth. Since they are accumulating over time, the question to know if the particles concentration become critical for the device arises.

From the specification data-sheet we read that the slit will first operate during 12 hours a day for two months (commissioning) and then 8 hours twice a week for 24 months. That means, for a frequence of 1.1Hz, the number of pulses will be: $3600 * (12 * 60 + 8 * 24 * 30 * 2/7) * 1.1 = 9.37.10^6$ pulses. Since one pulse deposits $9.96 \cdot 10^{13}$ particles, that makes $9.37.10^6 * 9.96 \cdot 10^{13} = 9.3 \cdot 10^{20}$ particles. The hydrogen distribution is given by SRIM, and is presented in appendix D. The volume where 95% of the particles deposits is about $(2 * 133.4 \cdot 10^5) * \pi * (2 * 236.7 \cdot 10^5)^2 = 1.88 \cdot 10^{23} A^3 = 0.19 cm^3$. This means the concentration of particles (at the point where they stop) in one half of slit is about $0.5 * 9.3 \cdot 10^{20} / 0.19 \simeq 2.34 \cdot 10^{21} particles/cm^3$. This value is very to the order of magnitude of usual atomic concentrations (table 4 page 24 of [4]). For carbons and graphites, the usual atomic density is about $10^{23} atoms/cm^3$ so that the relative amount of Hydrogen locked inside would be of 2%, i.e. not enough to modify the properties of graphite.

Moreover, diffusion may happen and reduce even more the concentration of hydrogen at that depth. Such diffusion has been observed for Helium [11].

Formation of hydrocarbons or other phases would then be limited and are likely not to impact on the function of the slit.

6.4 Shock waves

When the beam impacts on the slit, a shock wave is produced and then reflected on the edges. When the shock wave comes back in the middle, stresses might be critical and reached much higher level than those caused by the temperature gradient. [12].

However the evaluation of such stresses is not easy for complex shapes, and cannot be analytically driven. One easy solution is to introduce asymmetry in the design, by letting the beam impact not on the middle of the entrance surface of the slit, but slightly shifted to the right or the left with a distance in the order of magnitude of the radius of the beam (3 mm in our case).

That problem would need a whole thesis on its own to be fully treated.

6.5 Activation

There is no general and easy method to estimate the activation of the materials. A common rule of thumb is: the higher the atomic number the higher the activation.

A recently released program (2012), Actiwiz [1], developed by the CERN radioprotection team could help choose the low activation materials. Graphite and carbon composites are among them.

The final selection is left to the CERN radioprotection team. Graphite being a very used material in the field, nothing seems really to be feared.

6.6 Vacuum

The slit will work in Ultra-High Vacuum (UHV). Thus the less the material outgas the better. The quantities to evaluate the outgassing properties of the materials are:

- porosities proportion
- equilibrium vapor pressure
- adsorption and desorption properties

However there is no database for all material for those properties, therefore no selection can be driven.

The final materials selection has to be driven by the CERN vacuum team (VSC group). Graphite has already been used in such atmosphere [2].

6.7 Cost and maintenance

These two issues are common to all engineering projects, but are not crucial in the present case. However it is clear that the cheaper and the simpler the better.

[1] See url... but need CERN access.

6.8 Simulation with FLUKA and ANSYS

FLUKA [3] is a fully integrated particle physics MonteCarlo simulation package[2]. It is frequently used at CERN to evaluate the energy deposition of beams in matter. The present feasibility study depends on its validity, which we assume.

ANSYS [13] is a finite element software which uses the energy deposition profile given by FLUKA as input. The quality of the simulation mainly depends on:

- the relevance of the abstraction process
- the contacts
- the quality of the mesh[3]

The abstraction process reduces the problem to the simulation of the beam impacted volume. The simulation of the other parts, especially the copper jacket, or any screw or clamps are not relevant.

The convection coefficient used to simulate the cooling system is $5000W/m^2/K$, which is a typical value.

The shape of the slit being highly geometric (all the elements are perfect cubes), the quality of the mesh does not need any improvement.

2 See `http://www.fluka.org/fluka.php` for more details.

3 The quality of the mesh can be assessed by checking the proportion and deformation of its elements, the nodal fraction and difference.

7 Results and discussion

One predesign and one material have been identified. The last step to conclude on the feasibility of the slit is to run a simulation and check that:

- the maximal temperature remains below the working temperature of the predesign
- the maximal stress remains below the fatigue limit of the material
- the deformation of the slit remains below the specification limit ($50\mu m$)

The simulations of the interaction of the beam with matter are based on the FLUKA code [3]. The output file of FLUKA (deposition of energy) is the input file of the finite-element software ANSYS [13][1] (as a heat generation). The FLUKA simulation are shown on figure 7.4.

7.1 Temperature evolution

The evolution of the temperature at the Bragg peak position with time is presented on figure 7.1. The temperature in the slit at the 24th pulse is presented on figure 7.2.

From these two figures, two comments can be made. First, the maximal temperature reached is about $285°C$, that is much lower than the working temperature of graphite (which is about $2000°$). Secondly, the temperature on the external surface is low (below $60°C$) but not enough to consider any thermal dilatation of the jacket small.

The conclusion is that the predesign and the material pass the temperature test, but further investigation on the choice of the material for the jacket has to be considered.

7.2 Stresses

The fatigue safety factor is shown on figure 7.3. This factor is defined as the ratio of the Mohr-Coulomb stress in the material to the fatigue limit at 10^7 cycles[2]. Since the minimal value of the safety factor is above one (it is about 2), the set of the predesign and the material pass the stress test also.

From the specification data-sheet we read that the slit will first operate during 12 hours a day for two months (commissioning) and then 8 hours twice a week for 24 months. That means, for a frequence of 1.1Hz, the number of pulses will be: $3600 * (12 * 60 + 8 * 24 * 30 * 2/7) * 1.1 = 9.37.10^6$ pulses. We can therefore guarantee that this set of predesign and material will not mechanically fail for that time. Beyond it, the predesign and material should still fit for twice that time since the typical fatigue limit curves do not vary much after 10^7 cycles, but nothing is however sure.

7.3 Deformation

The final and maybe most important control is the deformation check. Indeed the purpose of the slit is precisely to keep its aperture stable during operation.

[1] The simulation launched was a transient thermal followed by a transient structural
[2] The value taken for the fatigue limit of graphite R4550 as input into ANSYS is taken from analogous graphites in CES.

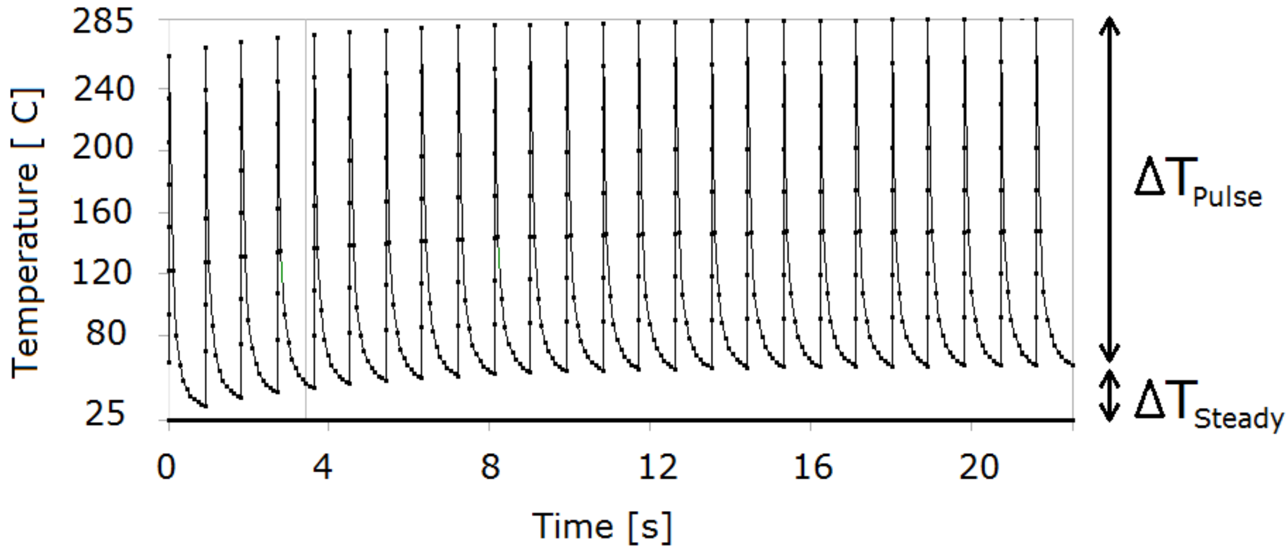

Figure 7.1.: Evolution of the temperature at the Bragg peak position during the first 25 pulses. ΔT_{pulse} corresponds to the variation of temperature caused by one pulse while $\Delta T_{SteadyState}$ corresponds to the remaining temperature after the heat of the pulse has been dissipated. After 25 pulses, this temperature becomes constant: the thermal equilibrium is reached. Graph made with ANSYS [13].

The deformation of the inner surfaces can also be evaluated by ANSYS, but in two steps. The calculation of the deformation at the thermal equilibrium with the input file from FLUKA takes too much computer time. To tackle that problem, we divided it in two small ones.

First the deformation due to one pulse can still be done by ANSYS in a reasonable time. The deformation of the slit following the first pulse is shown on figure 7.5 and is about $5\mu m$.

Secondly, the average deformation of the slit once the thermal equilibrium is reached can be approximated by considering that the beam energy is deposited along a small cylinder (see figure 7.6) This problem can also be solved by ANSYS, and lead to a value of the average deformation of $18\mu m$.

By summing the two components of the deformation, we get an approximation of the total deformation of the slit: $23\mu m$, which is below the value of $50\mu m$ which is given in the specification. Therefore the present set of predesign and material pass the deformation check.

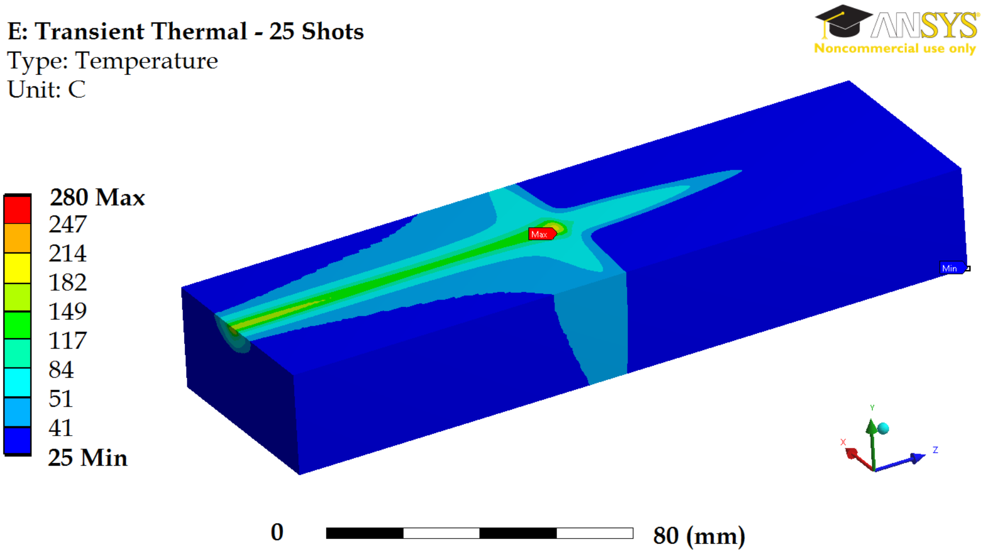

Figure 7.2.: Temperature in the slit at the 24th pulse. Figure made with ANSYS [13].

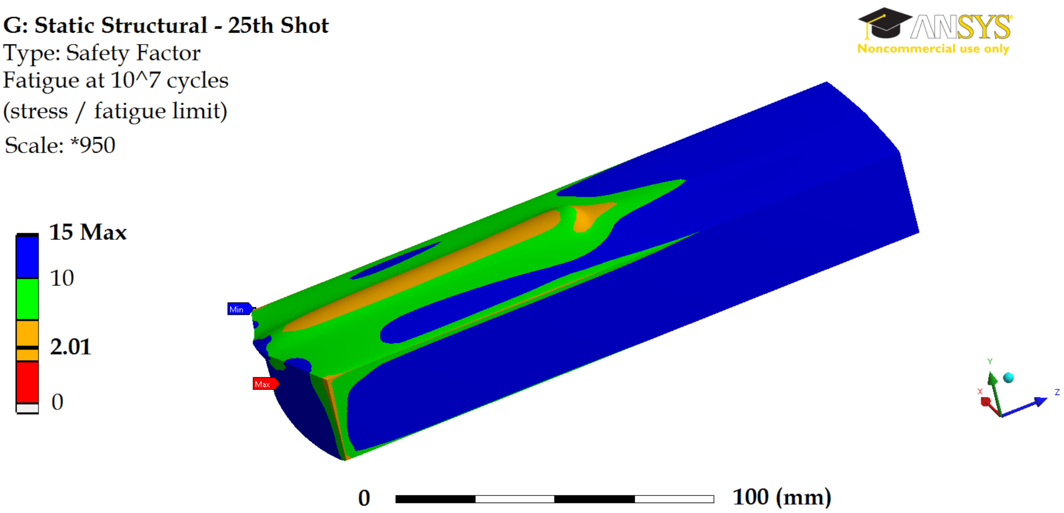

Figure 7.3.: Fatigue safety factor at 10^7 cycles. Because the safety factor is above 1, the predesign is safe. Figure made with ANSYS [13].

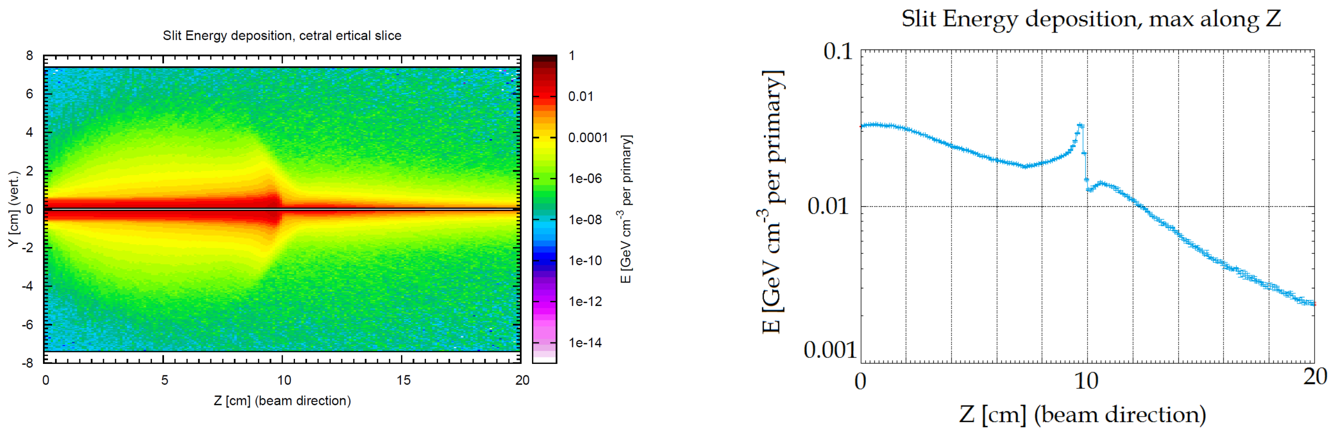

Figure 7.4.: Deposition of energy in the slit calculated by FLUKA [3] for graphite with a density of $2.2 g/cm^3$. On the left, the 2D map gives an idea of the significant volume of interaction of the beam with the slit. The yellow is already four orders of magnitude less than the peak of deposition of energy, i.e. more than 99.99% of the beam is in a cylinder with a radius of 3 cm. On the right, the maximal deposition of energy is about $0.035 GeV/cm^3$ at a depth of about 10cm.

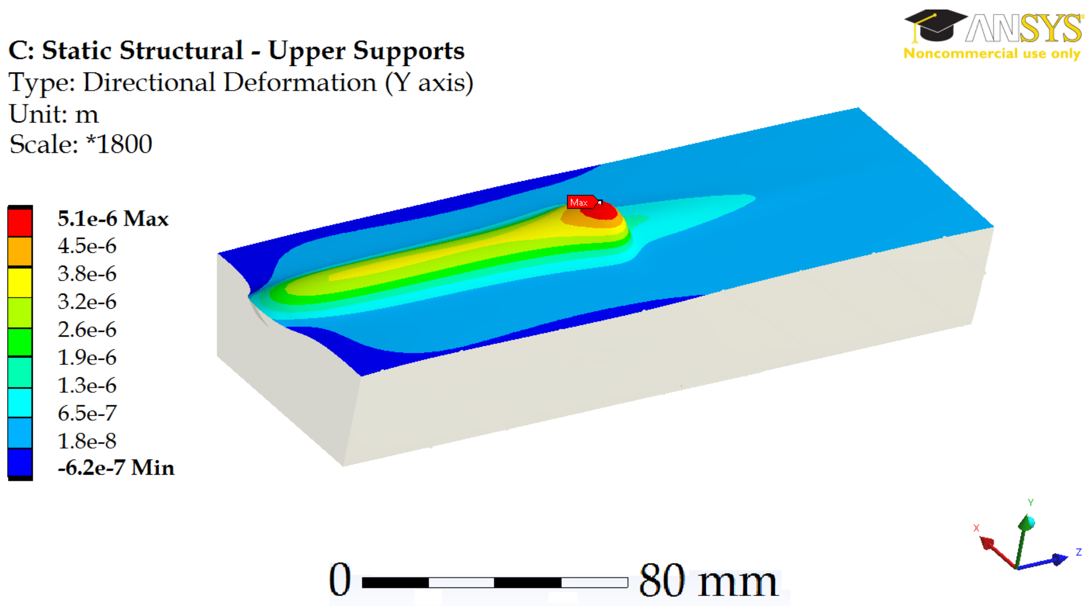

Figure 7.5.: Directional deformation of the inner surface of slit following the first pulse. The maximal deformation here is:$5 \mu m$. Figure made with ANSYS [13].

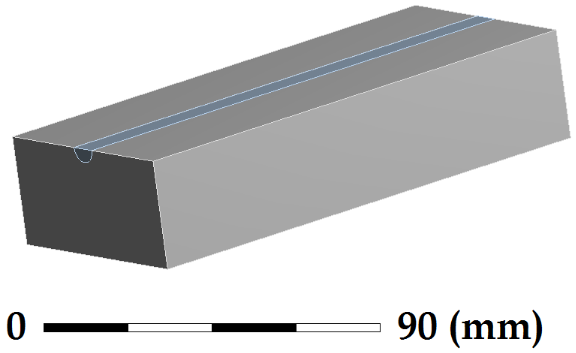

(a) Modelization of the slit in order to estimate the average deformation of the inner surface. The beam deposits a uniform energy along a cylinder in the middle.

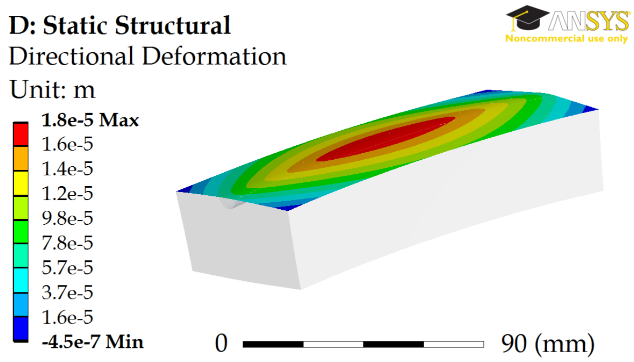

(b) Directional deformation of the slit based on the modelisation explained in paragraph 7.3. The maximal deformation here is: $18\mu m$.

Figure 7.6.: Evaluation of the average deformation of the slit when the thermal equilibrium is reached. The geometry is shown on the left: the volume of interaction of the beam with matter is assumed to be a cylinder. The heat deposition is assumed constant and equal to the maximal deposition of energy calculated by FLUKA: $0.035 GeV/cm^3$ as shown on figure 7.4. Figures made with ANSYS [13].

8 Conclusions

The slit is feasible from the thermal and mechanical point of view.

Once the problem has been clearly formulated and all the issues enumerated, a methodological approach has been defined. The key problem, deformation, and the key issues, temperature and stresses, were identified and treated thoroughly. The other issues were also tackled, but briefly.

The key problematic was to find the predesign and material that best suit the temperature, stresses and deformation issues. To tackle the problematic a systematic methodology was defined (section 3.4). Four steps were identified:

- Separation of predesign and material selection
- Predesign selection by literature review and imagination
- Selection of materials by figures of merit
- Finite element method as the concluding step

Two predesigns were proposed (sections 4.1 and 4.2) . Though both may be feasible, the first predesign was identified (figure 4.1) as the best one for simplicity reason.

Two figures of merit were then defined (paragraphs 5.1 and 5.1) to select the only possible materials. The class of graphites and carbons was found the best (figure 5.1). The only member of that class already in use at CERN is graphite R4550.

Finally, three finite-element simulation with FLUKA and ANSYS were launched to asses the temperature, stresses and deformation of the first predesign with graphite R4550. The results of the simulation show that the issues are met:

- The maximal temperature reached remain below the working temperature of graphite R4550
- The maximal stresses remain below the fatigue limit of graphite R4550
- The deformation remain below $50\mu m$ as the specifications stated

Most of the other issues are not critical, except maybe two: the microstructure evolution during irradiation and shock waves.

The choice was made to choose an amorphous materials to limit possible microstructure evolution which could eventually lead to significant evolution of the macroscopic properties of the materials (section 6.1).

The shock wave issue was dealt by introducing a slight dissymmetry in the predesign: the beam should not hit the slit right in the middle. A shift of 3mm to the right or left would already remove a concentration of stresses when the wave is reflected back in the middle (section 6.4).

Improvements are however far from impossible. First, other predesigns as simple as predesign 1 may exist. By changing the shape of the impacted area from perpendicular to "with an angle" (see table 4.1), stresses might be even lower. Secondly, the material chosen, graphite R4550, the best one in the set of available and already tested graphites at CERN. Other graphites or carbon composites might be better candidates. Finally, two issues should be investigated to reach a more satisfying predesign: the microstructure evolution during irradiation, and the propagation of shock waves in the slit.

The feasibility study being now closed, the next step consists in building the complete design so that to connect it to the other parts of the LBS line of the Linac 4.

A Specifications of the Slit and the beam

A.1 Introduction

The document at the origin of the slit feasibility study is the Linac 4 project document No L4-B-ES-0003 rev.0.3 supplied by the group BE/OP [14]. The EDMS (CERN document server) document number is 1094603. The main author is Thomas Hermanns (Thomas.Hermanns@cern.ch).

What follows sums up the relevant information and data for the present feasibility study.

A.2 Specifications

A.2.1 Beam pulse parameters

The paramters are given in table A.1. The beam intensity at the slit entrance has a gaussian shape with σ values of 2.8 mm (horizontal) and 2.2mm (vertical).

Table A.1.: Definitions of the Linac4 macro and micro pulses. A macro pulse is not a continuous stream of particles, but is structured in micro-pulses. The ion is H^- at 160 MeV

	Macro-Pulse	Micro-Pulse
Number of particles	$9.96 \cdot 10^{13}$	$1.14 \cdot 10^{9}$
Pulse length	$400\mu s$	$2.84ns$
Repetition rate	1.11 Hz	352.2 MHz
Average Current	40 mA	65 mA
Deposited energy per pulse	2.55 kJ	0.03 J

A.2.2 Slit parameters

- length : 200 mm at maximum, this corresponds to 2.4 times the absorption length of 160 Mev H^- in carbon. Other materials, or smaller length can be proposed.
- aperture size : 1mm x 148 mm. A precision of $50\mu m$ is tolerable.
- position and angular aligment precision : 0.15 mm precision for horizontal and vertical aligment should not be exceeded.

A.2.3 Operational scenarios

Not one but several scenarios should be considered for the LBS line. Table A.2 sums up the four scenarios.

Table A.2.: Operational scenarios for H^- at 160 MeV

Scenario	Average current	Pulse length	Repetition rate	Mean Power	comments
Commissioning	40 mA	100 μs	1.11 Hz	709 W	12h per day
Measurement operation	40 mA	100 μs	0.1* 1.11 Hz	71 W	$\simeq$ 8h, twice per week during 24 months (max LHC run)
MD	40 mA	400 μs	0.1* 1.11 Hz	283 W	10 single shots without interlock
Failure	40 mA	400 μs	1.11 Hz	2830 W	2 consecutive shots, before interlock sets in

A.2.4 Other requirements

Vacuum level of less than $10^{-8} mbar$ without the beam has to be maintained. That means the vapor pressure of the slit should be as low as possible.
Activation of the slit is expected. Radiation and activation simulations should be performed to identify the shielding needs in the vicinity of the slit.

B ΔT_{pulse} model

The definition of the figures of merit for material selection of section 5.1 needs the development of the present model.

The model evaluates the increase of temperature following a pulse where the maximum increase is expected.

The maximum increase of temperature is expected either on the entrance surface or at the Bragg peak. The model then evaluates the increase of temperature at these two points (equations 9 and 13, 20 and 21).

Two versions of the model are proposed. The first one is valid for all energy below 200 MeV but need the SRIM software (equation 9 and 13). The second version is only valid for 160MeV but does not need SRIM (equation 20 and 21).

The model develops a conservative approach and estimates the maximal increase of temperature possible. It gives an upper bound of the temperature reached.

The model is voluntarily left to the format of a paper and is sufficient to itself. The reference are not included, they are limited to two: SRIM [7] and FLUKA [3].

A model for the determination of the maximal increase of temperature in a 160 MeV proton beam intercepting device following the first pulse

A. Ouzia

Abstract

The aim of this study is to evaluate the maximal temperature reached in a beam intercepting device (BID) right after the first beam pulse. The beam considered here is a 160 MeV proton beam (Linac 4 beam).

Two versions of the model are proposed. The first, requires values calculated by SRIM whereas the second, (less precise) only relies on the properties on the material. The model considers that the entire beam power is transformed into heat and therefore develops a conservative approach.

Keywords: Linac 4, maximal increase of temperature, beam pulse, beam intercepting devices, SRIM

1 Introduction

Upon irradiation by energetic protons, beam intercepting devices heat and deform leading to internal stresses. Such stresses might cause the failure of the device and are a common problem in the realisation of beam intercepting devices.

The order of magnitude of such stresses directly depends on the heat generated, which depends on the energy deposition. The properties of the material impacts on the amount of heat generated and the resulting internal stresses. Some materials may heat less than other but still fail due to resulting stresses higher than their yield strength. Some other may heat more but having much better thermal and mechanical properties, they will not fail. Therefore the question is not to know what materials heat less than others or what materials have better mechanical properties than the other but what materials have the best compromise.

The choice of the materials should therefore take into account this compromise, this is one aspect of the present model. Figures of merit using the results of the model can then target the only set of possible materials for such a beam.

2 Formulation and modelization of the problem

2.1 First description of the problem

2.1.1 Case of one particle

When an energetic particle penetrates a beam intercepting device (BID), it loses its energy and therefore gradually slows until it stops (assuming the BID is long enough). The term describing the energy loss is called the stopping power and is denoted $\frac{dE}{dz}$ where z is the depth

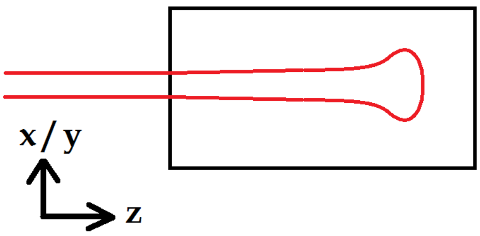

(a) *Illustration of the particle trajectory in matter. The distribution of the particles evolves with depth, especially close to the end of the pathway. The red lines represent the volume in which 99.99 % of the particles are (the beam distribution is a gaussian).*

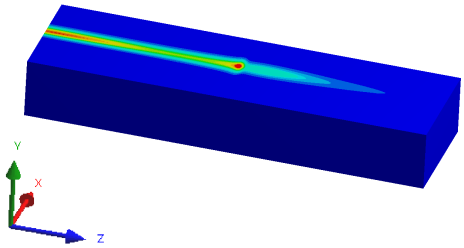

(b) *Temperature in half of a slit following the first shot of 160 MeV protons in graphite. The maximal temperatures are reached in two regions: in the first mm and at a given depth. The simulation was run with ANSYS 13 using the FLUKA code to simulate the beam interaction with matter.*

Figure 1 – *Illustrations of the beam trajectory (left) and resulting temperature in the material following the first shot (right).*

axis. The energy deposition can either be solved with the Bethe-Bloch equation or using a Monte-Carlo code such as SRIM (Stopping and Range of Ions in Matter) [1] or FLUKA[2].

When the particle penetrates matter it does not travel along a straight trajectory. It will deviate from its trajectory due to interaction with matter. This is called straggling (longitudinal or lateral).

2.1.2 Case of one beam

By contrast with a particle, one beam already has a spatial distribution when it hits the dump. All particles are not concentrated on one point but are distributed in space according to a gaussian distribution. When it enters matter, each particle has its own trajectory leading to the spread of the distribution with depth[3] (illustrated on figure 1a).

The deposition of energy occurs according to several mechanisms, among which electronic losses are one of the main for energies up to 200 MeV. Other mechanisms include nuclear interactions. Electronic losses results in the heating of the material.

2.1.3 Reformulation of the problem

The first question is where does the maximum of heat deposition happen. At first sight the Bragg peak might seem the only candidate. However the beam experiences straggling: the beam distribution dilutes with depth (see figure 3 and 4). The beam distribution may well be diluted enough at the Bragg peak so that the maximal heat deposition occurs at the entrance surface where the beam is well focused, thus:

> "The maximal energy deposition occurs either at the Bragg peak OR at the entrance surface "

The problem is therefore:

> "What is the increase of temperature at the entrance surface and at the Bragg peak "

[1]SRIM is a collection of software packages which calculate many features of the transport of ions in matter. Ion stopping and ranges in targets is a typical applications. For more details see `http://www.srim.org/`

[2]FLUKA is a fully integrated particle physics MonteCarlo simulation package. It has many applications in high energy experimental physics and engineering, shielding, detector and telescope design, cosmic ray studies, dosimetry, medical physics and radio-biology. For more details see `http://www.fluka.org/fluka.php`

[3]and interaction between the particles also occurs

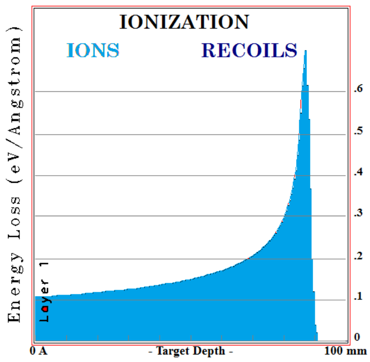

(a) *Average deposition of energy of one 160 MeV protons in carbon. The peak of deposition is called the Bragg peak and is where the maximum of temperature would be reached if only one particle was sent. (simulation made with SRIM)*

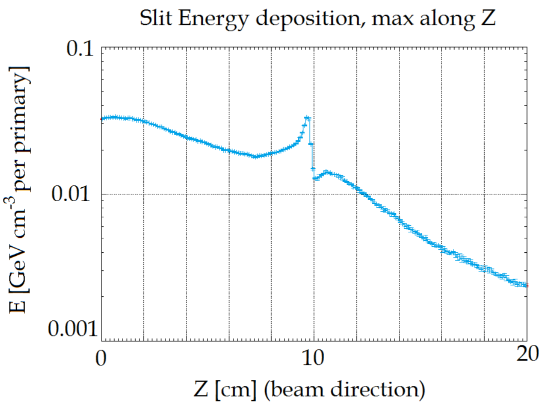

(b) *Deposition of energy of a beam of 160 MeV protons (Linac 4 beam) in graphite (the trajectory is seen in figure 1b). By contrast with one particle a peak of energy deposition occurs at the entrance surface.(simulation made with FLUKA)*

Figure 2 – *Comparison of the deposition of energy for one particle (left) and for a beam (right).*

Once calculated, the highest one gives the maximal increase of temperature.

2.2 Modelisation and approach

The volume where more than 99% of the beam is intercepted has the shape given in figure 1a. This volume is considered to be cut into discs of thickness ϵ, so that ϵ is small enough compared to any variation of the temperature along the z axis.

We will focus on two specific discs: the first one at the entrance surface and the one at the Bragg peak depth. The approach is:

- to determine the distribution of deposited energy in the discs $D_{entrance}$ and D_{Bragg}
- to determine the energy deposited in each disc
- to determine the energy deposited in a small prism situated at the center of the disc
- get ΔT from reformulation of the first principle of thermodynamics (see section 3.1)

3 Data and relations known

3.1 Thermodynamical relation

The Linac 4 beam is considered. One pulse deposits $E_{tot}^{deposited} = 2.55kJ$ The beam shot is considered short enough ($400\mu s$) to assume there is no heat dissipation during the time of impact. Moreover the whole beam power is considered to be absorbed as heat [4].

Under these assumption, the first principle can be written:

$$\delta Q + \delta W = dU = dE_{deposited} \tag{1}$$

[4] This means we only take into account the electronic losses (which in the end results in heat). Nuclear reactions may actually not be negligible but there are no easy rule to have an order of magnitude of these. Below 200MeV, it is common knowledge that the main part of the energy deposition consist of electronic interactions. Therefore the worst case is considered here.

where $E_{deposited}$ is the energy deposited by the beam. Assuming their is no mechanical work ($\delta W = 0$):

$$\delta Q + \delta W = \delta Q = C_p \Delta T = dU = E_{deposited}$$

where C_p is the specific heat of the material of the dump. By introducing the specific heat of the material c_p such that $C_p = mc_p$ where m is the mass of the material interacting with the dump, the previous equation becomes:

$$mc_p \Delta T = E_{deposited}$$

dividing both side by the volume V of material interacting with the dump, we get:

$$\frac{m}{V} c_p \Delta T = \frac{E_{deposited}}{V}$$

which finally reduces to:

$$\boxed{\rho c_p \Delta T = \frac{E_{deposited}}{V}} \tag{2}$$

3.2 Beam parameters

The beam considered here is a 160 MeV Proton beam with $9.96 \cdot 10^{13}$ particles/pulse (Linac 4 beam). The energy of 1 pulse is $2553J$. It has a beam distribution $\sigma_x = 2.2mm$ and $\sigma_y = 2.8mm$ Figures **??** represents one beam shot.

4 Calculation details

4.1 Method using SRIM

4.1.1 Entrance surface disc

At the entrance surface, one particle deposits an energy which can be read on SRIM: $\left.\frac{dE}{dz}\right|_{z=0}$.
The energy deposited in the surface disk of thickness ϵ is:

$$E_{disc}^{z=0} = N_{particules} \left.\frac{dE}{dz}\right|_{z=0} \epsilon \tag{3}$$

where $N_{particules}$ is the number of particles in one beam shot.

The proportion α of the beam going through the small prism $\sigma_x/10 \cdot \sigma_y/10 \cdot \epsilon$ [5], situated at the center of the disc, to the entire disc is:

$$\alpha = \frac{\int\limits_{-\sigma_x/20}^{\sigma_x/20} \int\limits_{-\sigma_y/20}^{\sigma_y/20} \int\limits_{0}^{\epsilon} d(x,y,z) dxdydz}{\int\limits_{-\infty}^{\infty} \int\limits_{-\infty}^{\infty} \int\limits_{0}^{\epsilon} d(x,y,z) dxdydz} \tag{4}$$

where $d(x, y, z)$ is the beam spatial distribution, i.e. a gaussian, so that:

$$\alpha = \frac{\int\limits_{-\sigma/20}^{\sigma/20} \int\limits_{-\sigma/20}^{\sigma/20} \int\limits_{0}^{\epsilon} e^{-\left(\frac{x^2}{2\sigma_x^2} + \frac{y^2}{2\sigma_y^2}\right)} dxdydz}{\int\limits_{-\infty}^{\infty} \int\limits_{-\infty}^{\infty} \int\limits_{0}^{\epsilon} e^{-\left(\frac{x^2}{2\sigma_x^2} + \frac{y^2}{2\sigma_y^2}\right)} dxdydz} \tag{5}$$

[5] the σ is the parameter of the gaussian distribution describing the beam. $sigma_{x/y}/10$ was chosen since the beam distribution barely changes on this range

since $e^{-\left(\frac{x^2}{2\sigma^2}\right)} \simeq 1$ in the range $[-\sigma/20;\sigma/20]$ and the integral of a gaussian is $\sqrt{2\pi\sigma^2}$, the previous equation becomes:

$$\frac{\sigma_x/10 \cdot \sigma_y/10 \cdot \epsilon}{\sqrt{2\pi\sigma_x^2}\sqrt{2\pi\sigma_y^2} \cdot \epsilon} = \alpha$$

so that finally:

$$\alpha = \frac{1}{200\pi} \tag{6}$$

Therefore the total energy deposited in the prism is:

$$E_{prism} = \alpha E_{disc}^{z=0} \tag{7}$$

$$= \alpha N_{particules} \cdot \left.\frac{dE}{dz}\right|_{z=0} \epsilon \tag{8}$$

and using equation 2:

$$\Delta T_{surface} = \frac{1}{\rho c_p}\frac{E_{prism}}{V_{prism}}$$

$$= \frac{1}{\rho c_p} \cdot \frac{\alpha N_{particules} \cdot \left.\frac{dE}{dz}\right|_{z=0} \cdot \epsilon}{\sigma_x/10 \cdot \sigma_y/10 \cdot \epsilon}$$

finally:

$$\boxed{\Delta T_{surface} = \frac{1}{\rho c_p} \cdot \frac{N_{particules} \cdot \left.\frac{dE}{dz}\right|_{z=0}}{2\pi \cdot \sigma_x \cdot \sigma_y}} \tag{9}$$

4.1.2 Bragg peak disk

By contrast with the previous case, the beam spatial distribution $d(x, y, z = z_{Bragg})$ is different to the original distribution. The cause is the straggling of the particles when they interact with matter. This is illustrated on figure 3. We therefore introduce the quantity σ_s to describe the gaussian distribution of one particle at the Bragg peak depth.

What is then the distribution in the Bragg peak plane ? Considering a flow of particle going through $(X_i, Y_i, 0)$ (see figure 4), the flow will spread to a gaussian distribution at the Bragg peak:

$$\frac{e^{-\left(\frac{(x-X_i)^2+(y-Y_i)^2}{2\sigma_s^2}\right)}}{2\pi\sigma_s^2} \tag{10}$$

and the distribution of particle at point $(X_i, Y_i, 0)^6$ is:

$$d(X_i, Y_i, z = 0) = \frac{N_{particules}}{2\pi\sigma_x\sigma_y} \cdot e^{-\left(\frac{(X_i)^2}{2\sigma_x^2}+\frac{(Y_i)^2}{2\sigma_y^2}\right)}$$

so that the distribution of particles at (x, y, z_{Bragg}) is the product of the two:

$$d(x, y, z_{Bragg}, X_i, Y_i) = \frac{N_{particules}}{2\pi\sigma_x\sigma_y} \cdot e^{-\left(\frac{(X_i)^2}{2\sigma_x^2}+\frac{(Y_i)^2}{2\sigma_y^2}\right)} * \frac{e^{-\left(\frac{(x-X_i)^2}{2\sigma_s^2}+\frac{(y-Y_i)^2}{2\sigma_s^2}\right)}}{2\pi\sigma_s^2}$$

The total distribution in the Bragg peak plane is obtained by integration over X_i and Y_i:

[6] Please note that x and y refer to the plane at z_{Bragg} while X_i and Y_i refer to positions at the entrance surface plane

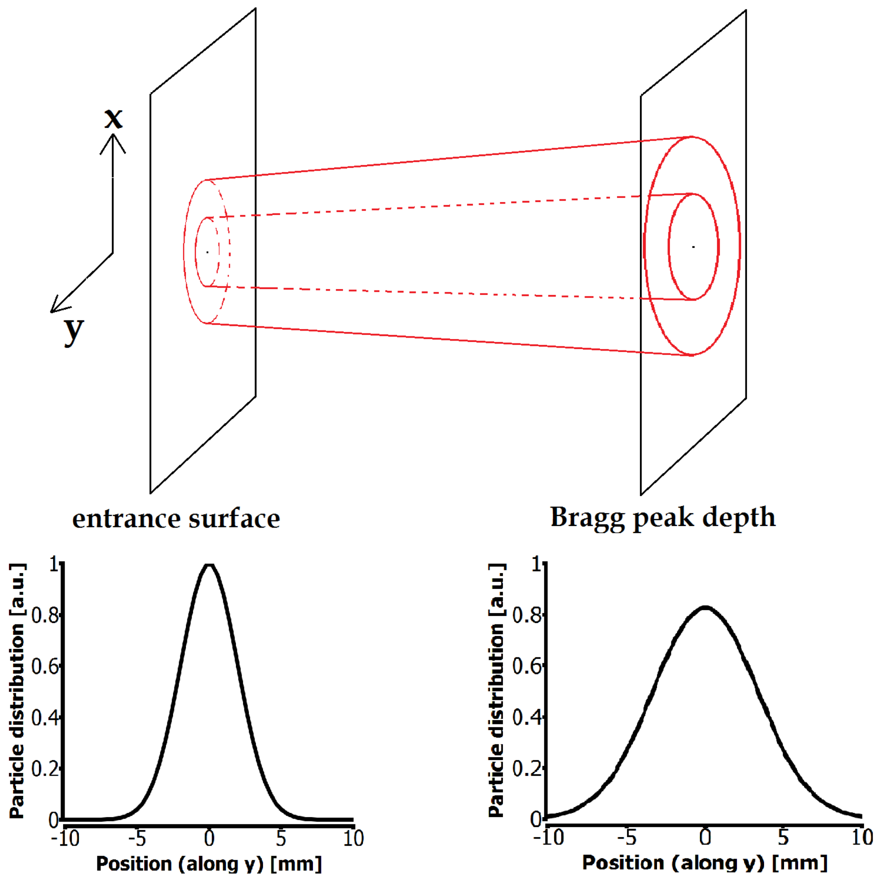

Figure 3 – *Beam particle distribution in the surface and Bragg peak planes. Because of interaction between the incoming protons and matter, straggling occurs and the distribution flattens. Both distribution are gaussian as it is proved in section 4.1.2.*

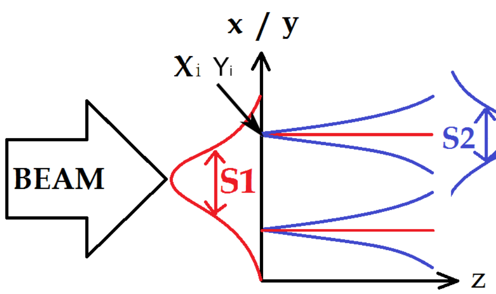

Figure 4 – *Beam particle distribution in the surface and Bragg peak planes. Because of interaction between the incoming protons and matter, straggling occurs and the distribution flattens. Both distribution are gaussian as it is proved in section 4.1.2.*

$$d(x,y,z_{Bragg}) = \frac{N_{particules}}{2\pi\sigma_x\sigma_y} * \frac{1}{2\pi\sigma_s^2} * \int_{-\infty}^{\infty}\int_{-\infty}^{\infty} e^{-\left(\frac{(X_i)^2}{2\sigma_x^2}+\frac{(Y_i)^2}{2\sigma_y^2}\right)} * e^{-\left(\frac{(x-X_i)^2}{2\sigma_s^2}+\frac{(y-Y_i)^2}{2\sigma_s^2}\right)} dX_i dY_i$$

Since the integration is symmetric in x and y,we can focus only on the resolution of:

$$A = \int_{-\infty}^{\infty} e^{-\frac{X_i^2}{2\sigma_x^2}-\frac{(x-X_i)^2}{2\sigma_s}} dX_i$$

Using Maple, we get:

$$A = \frac{2\sqrt{\pi}}{\sqrt{\frac{2}{\sigma_x^2}+\frac{2}{\sigma_s^2}}} \cdot exp\left(-\frac{x^2}{2\sigma_x^2} - \frac{x^2}{4\sigma_x^4\left(-\frac{1}{2\sigma_x^2}-\frac{1}{2\sigma_s^2}\right)}\right)$$
$$= \frac{2\sqrt{\pi}}{\sqrt{\frac{2}{\sigma_x^2}+\frac{2}{\sigma_s^2}}} \cdot exp\left(-x^2(\frac{1}{2\sigma_x^2} + \frac{1}{4\sigma_x^4\left(-\frac{1}{2\sigma_x^2}-\frac{1}{2\sigma_s^2}\right)})\right)$$

let σ_{eq_x} such that:

$$\frac{1}{\sigma_{eq_x}^2} = \frac{1}{2\sigma_x^2} + \frac{1}{4\sigma_x^4\left(-\frac{1}{2\sigma_x^2}-\frac{1}{2\sigma_s^2}\right)} = \frac{1}{2\sigma_x^2} - \frac{1}{4\sigma_x^4\left(\frac{1}{2\sigma_x^2}+\frac{1}{2\sigma_s^2}\right)}$$

after full calculation, we come to:

$$\sigma_{eq_x}^2 = \sigma_x^2 + \sigma_s^2 \tag{11}$$

thus A can be rewritten:

$$A = \frac{2\sqrt{\pi}}{\sqrt{\frac{2}{\sigma_x^2}+\frac{2}{\sigma_x^2}}} \cdot exp(-\frac{x^2}{2(\sigma_x^2+\sigma_s^2)}) = \sqrt{\frac{2\sigma_x^2\sigma_s^2\pi}{\sigma_x^2+\sigma_s^2}} \cdot exp(-\frac{x^2}{2(\sigma_x^2+\sigma_s^2)})$$

and coming back to equation , we have:

$$\int_{-\infty}^{\infty}\int_{-\infty}^{\infty} e^{-\left(\frac{(X_i)^2}{2\sigma_x^2}+\frac{(Y_i)^2}{2\sigma_y^2}\right)} * e^{-\left(\frac{(x-X_i)^2}{2\sigma_x^2}+\frac{(y-Y_i)^2}{2\sigma_y^2}\right)} dX_i dY_i = \sqrt{\frac{2\sigma_x^2\sigma_s^2\pi}{\sigma_x^2+\sigma_s^2}} \cdot \sqrt{\frac{2\sigma_y^2\sigma_s^2\pi}{\sigma_y^2+\sigma_s^2}}$$
$$exp(-\frac{x^2}{2(\sigma_x^2+\sigma_s^2)})exp(-\frac{y^2}{2(\sigma_y^2+\sigma_s^2)})$$

$$= \sqrt{\frac{2\sigma_x^2\sigma_s^2\pi}{\sigma_{eq_x}}} \cdot \sqrt{\frac{2\sigma_y^2\sigma_s^2\pi}{\sigma_{eq_y}}} exp(-\frac{x^2}{2\sigma_{eq_x}})exp(-\frac{y^2}{2\sigma_{eq_y}})$$

thus:

$$d(x,y,z_{Bragg}) = \frac{N_{particules}}{2\pi\sigma_x\sigma_y} * \frac{1}{2\pi\sigma_s^2} * \sqrt{\frac{2\sigma_x^2\sigma_s^2\pi}{\sigma_{eq_x}}} \cdot \sqrt{\frac{2\sigma_y^2\sigma_s^2\pi}{\sigma_{eq_y}}} exp(-\frac{x^2}{2\sigma_{eq_x}})exp(-\frac{y^2}{2\sigma_{eq_y}})$$

and finally:

$$d(x,y,z_{Bragg}) = \frac{1}{2\pi(\sigma_{eq_x}^2+\sigma_{eq_y}^2)} \cdot exp\left(-\frac{x^2}{2\sigma_{eq_x}^2} - \frac{y^2}{2\sigma_{eq_y}^2}\right) \tag{12}$$

where:

- $\sigma_{eq_x}^2 = \sigma_x^2 + \sigma_s^2$
- $\sigma_{eq_y}^2 = \sigma_y^2 + \sigma_s^2$

Similarly to paragraph 4.1.1, α is independant of the variance of the gaussian (σ) so that the proportion of the beam going through the small prism $\sigma_{eq_x}/10 \cdot \sigma_{eq_y}/10 \cdot \epsilon$ is also $\alpha = 1/(200\pi)$. The equation describing the increase of temperature is therefore very similar shape to equation 9:

$$\boxed{\Delta T_{Bragg} = \frac{1}{\rho c_p} \cdot \frac{N_{particules} \cdot \left.\frac{dE}{dz}\right|_{Bragg}}{2\pi \cdot \sigma_{eq_x} \cdot \sigma_{eq_y}}} \tag{13}$$

4.1.3 Comparison between $\Delta T_{Surface}$ and ΔT_{Bragg}

It might be useful to see at one glance whether the maximal increase of temperature will occur at the surface of the Bragg peak depth. Here we give a rule of thumb:

$$\frac{\Delta T_{Bragg}}{\Delta T_{Surface}} = \frac{\left.\frac{dE}{dz}\right|_{Bragg}}{\left.\frac{dE}{dz}\right|_{Surface}} * \frac{\sigma_x \cdot \sigma_y}{\sigma_{eq_x} \cdot \sigma_{eq_y}} = E * \frac{\sigma_x \cdot \sigma_y}{\sigma_{eq_x} \cdot \sigma_{eq_y}}$$

For 160 Mev, $E \simeq 6$ for all materials (it has been assessed with SRIM), so that:

$$\frac{\Delta T_{Bragg}}{\Delta T_{Surface}} = 6 * \frac{\sigma_x \cdot \sigma_y}{\sqrt{\sigma_x^2 + \sigma_s^2}\sqrt{\sigma_y^2 + \sigma_s^2}} = \frac{6}{\sqrt{1 + \frac{\sigma_s^2}{\sigma_x^2}}\sqrt{1 + \frac{\sigma_s^2}{\sigma_y^2}}} \tag{14}$$

Since $sigma_x$ and $sigma_y$ are usually close: $\sigma_x \simeq \sigma_y \simeq \sigma$ the equation becomes:

$$\frac{\Delta T_{Bragg}}{\Delta T_{Surface}} = 6 * \frac{\sigma_x \cdot \sigma_y}{\sqrt{\sigma_x^2 + \sigma_s^2}\sqrt{\sigma_y^2 + \sigma_s^2}} = \frac{6}{1 + \frac{\sigma_s^2}{\sigma^2}}$$

which means ΔT_{Bragg} predominates over $\Delta T_{Surface}$ if and only if $6 > 1 + \frac{\sigma_s^2}{\sigma^2}$, i.e. $\sigma_s < \sqrt{5}\sigma \simeq 2.25\sigma$[7]

4.2 Method without using SRIM

4.2.1 Dangers and usefulness of this method

In the equation 9 and 13, SRIM was used to get $\frac{dE}{dz}$ at the surface and the Bragg Peak positions. Moreover the radial straggling of the beam was taken from it to get equation 13, since $\sigma_{eq_x}^2 = \sigma_x^2 + \sigma_s^2$.

Another way has to be found to estimate $\left.\frac{dE}{dz}\right|_{z=0}$ and $\left.\frac{dE}{dz}\right|_{Bragg}$ and σ_s. It was found that correlation could indeed be found between these quantities and the intrinsic properties of the materials (ρ, c_p and Z as we will see).

However these estimations are only approximate at 160 MeV protons, and are based on SRIM. They will therefore only give the right order of magnitude, but not the right value.

The usefulness of the method lays in the fact that ΔT is connected only to the intrinsic properties of the material and the beam. Figures of merit can therefore be derived from this estimation and classify all the candidate materials [8]

[7] For 160MeV protons, $\sigma_s \simeq 2mm \pm 1mm$ for most materials. Therefore the maximal increase of temperature is at the Bragg peak for beam with $\sigma > 2mm$.

[8] The CES software can rank materials according to one properties or a composition of these, such as a figure of merit. Once we have a figure of merit, this software proves extremely useful.

4.2.2 Estimation of the range and the straggling

From the SRIM software, the following correlations where assessed for positive protons at 160 MeV:

$$R[m] = \frac{50.82}{\rho[kg/m^3]^{0.814}} \tag{15}$$

$$S[m] = R \cdot \left[\frac{\sqrt{Z\rho R}}{K_s}\right]^{\frac{1}{1.05}} = 0.25 \cdot \frac{Z^{\frac{1}{2.2}}}{\rho \cdot 73} \tag{16}$$

where R is the average range (in meters) of the protons and S the σ of the gaussian describing the scattering of an infinitely thin beam (in meters also). Z is the atomic number of the material[9] and K_s is a constant which is determined in the calculation details section. The correlation coefficients for R and S are respectively .992 and 0.96.

In order to get $\left.\frac{dE}{dz}\right|_{z=0}$ and $\left.\frac{dE}{dz}\right|_{Bragg}$ from R (the Range), the quantity $\left.\frac{dE}{dz}\right|_{Average}$ is introduced:

$$\left.\frac{dE}{dz}\right|_{Average} = \frac{E_{1particle}}{Range} = \frac{160MeV}{R} \tag{17}$$

From this quantity, the following correlations were made:

$$C = \frac{\left.\frac{dE}{dz}\right|_{Bragg}}{\left.\frac{dE}{dz}\right|_{Average}} \simeq 3.88 \tag{18}$$

$$D = \frac{\left.\frac{dE}{dz}\right|_{z=0}}{\left.\frac{dE}{dz}\right|_{Average}} \simeq 0.6 \tag{19}$$

The standart deviation of C and D are respectively of 0.1 and 0.01. Injecting these relations in equations 13 and 9:

$$\boxed{\Delta T_{surface} = \frac{1}{\rho^{0.186} c_p} \cdot \frac{3.02.10^{-13} \cdot N_{particules}}{2\pi \cdot \sigma_x \cdot \sigma_y}} \tag{20}$$

$$\boxed{\Delta T_{Bragg} = \frac{1}{\rho^{0.186} c_p} \cdot \frac{1.92.10^{-12} \cdot N_{particules}}{2\pi \cdot \sigma_{eq_x} \cdot \sigma_{eq_y}}} \tag{21}$$

where:

- $\sigma_{eq_x}^2 = \sigma_x^2 + \sigma_s^2$
- $\sigma_{eq_y}^2 = \sigma_y^2 + \sigma_s^2$

or to put it in its fully developped form:

$$\boxed{\Delta T_{Bragg} = \frac{1}{\rho^{0.186} c_p} \cdot \frac{1.92.10^{-12} \cdot N_{particules}}{2\pi \cdot \sqrt{\sigma_x^2 + \left(.25 \cdot \frac{Z^{\frac{1}{2.2}}}{\rho \cdot 73}\right)^2} \cdot \sqrt{\sigma_x^2 + \left(.25 \cdot \frac{Z^{\frac{1}{2.2}}}{\rho \cdot 73}\right)^2}}} \tag{22}$$

From the previous two equations comments can be made:

[9] or the average weighted atomic mass if this is a compound

- since the denominator of equation 21 is in the order of magnitude of 1, ΔT will be in the order of the magnitude of a few Kelvins if the numerator is also of the order of magnitude of 1, i.e. if $N_{particles} * 1.95.10^{-12} \simeq 1$ i.e. $N_{particles} \simeq 5.10^{11}$. This gives an order of magnitude of the number of particles in one pulse from which the "temperature" really increases.

- the importance of the density of the material relatively to the maximal increase of temperature is VERY small since its exponent is small. It is interesting to notice that the only intrinsic property of the material relevant here is the specific heat capacity.

5 Critics of the model

5.1 Limits and sources of errors

The two main sources of errors are:

- the assumption that the entire beam energy is transformed into heat. In reality, when nuclear reactions occur, some particles are produced and some escape from the material, but not everything is converted to heat.

- SRIM's own limitations. It explicitely appear in equations 13 and 9, but is hidden in 21 and 20 through correlations made.

Comparisons were made with FLUKA for this energy (160 MeV) and no significant difference were found (the values obtained are in the same order of magnitude). The present model gives values systematically higher than those obtained from FLUKA. This is probably due to nuclear interactions not taken into account in the present model. Yet by applying a coefficient of 2/3 to all our results, the results were as close as 20% (standard deviation) to those of FLUKA.

5.2 On the generalisation to other beam energies

The question should be asked whether such model could be generalized to other beam energies.

The rigorous answer is NO. However the method used to reach such results remains valid for beam energies lower than 160 MeV at least. Above such energy, nuclear interactions may be far from negligible, ruining the relevance of the model.

Even if the model can not be generalized to other energies, it provides valuable results which are at first sight counter intuitive. It is sometimes thought that the higher the density the higher the temperature reached. However equation 21 and 20 proves that it is not the case in general.

C Datasheet of Graphite R4550

The data below are based on tests made at CERN.

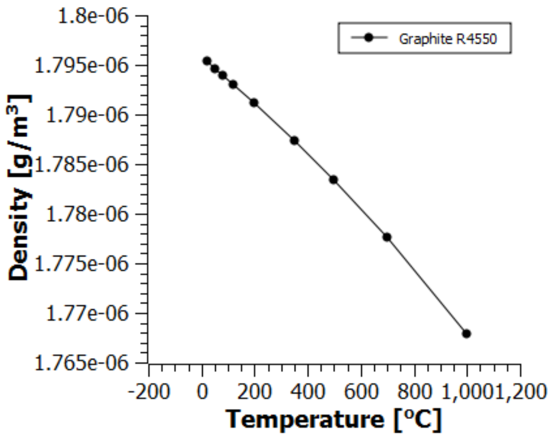

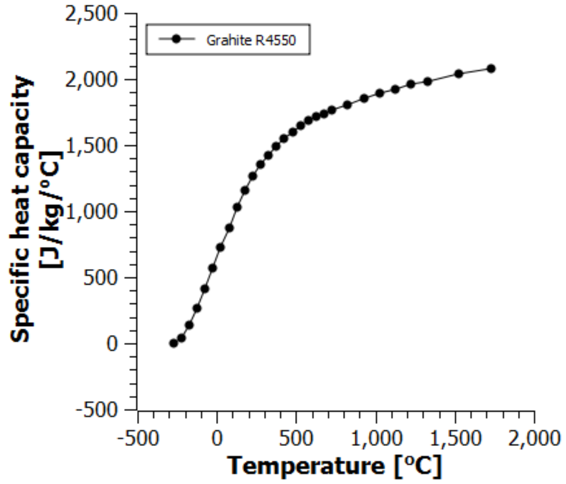

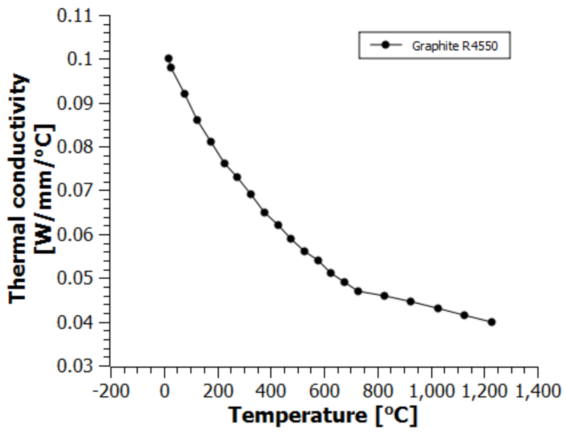

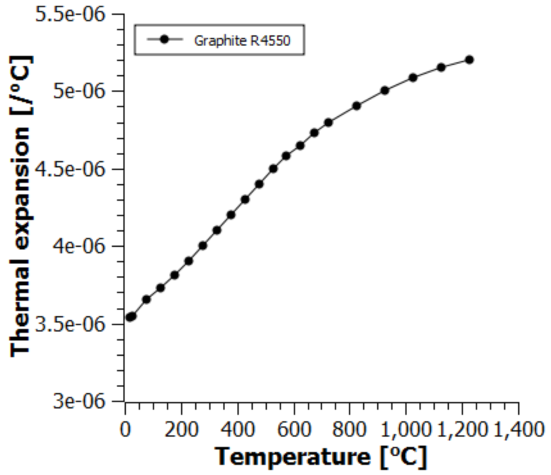

Table C.1.: Mechanical properties of Graphite R4550

Properties	Numerical value	Unit
Young's modulus	11500	MPa
Poisson's ratio	0.1	no unit
Bulk modulus	4791.7	MPa
Shear modulus	5227.3	MPa
Tensile Yield Strength	38	MPa
Compressive Yield Strength	125	MPa

D Distribution of Hydrogen with depth

This is the simulation of the distribution of the Hydrogen ions in the slit. SRIM [7] was used for the purpose.

```
====== H (10) into Layer 1                      =======
        SRIM-2008.04
==================================================
      ION and final RECOIL ATOM Distributions
 See  SRIM Outputs\TDATA.txt for calculation details
==================================================
 Ion     =  H   Energy = 160000  keV
============= TARGET MATERIAL ======================================
Layer   1 : Layer 1
Layer Width =     1.E+09 A   Layer # 1- Density = 9.024E22 atoms/cm3 = 1.8 g/cm3
  Layer # 1-  C = 100  Atomic Percent = 100  Mass Percent
====================================================================
 Total Ions calculated =4466.00
 Ion Average Range =   109.3E+07 A   Straggling =   133.4E+05 A
 Ion Lateral Range =   150.4E+05 A   Straggling =   223.1E+05 A
 Ion Radial  Range =   236.7E+05 A   Straggling =   196.1E+05 A
====================================================================
 Transmitted Ions =;  Backscattered Ions =1
 (These are not included in Skewne- and Kurtosis below.)

 Range Skewne- = -000.5701  &= [-(X-Rp)^3]/[N*Straggle^3]
 Range Kurtosis = 007.4305  &= [-(X-Rp)^4]/[N*Straggle^4]
 Statistical definitions above are those used in VLSI implant modelling.
====================================================================
```

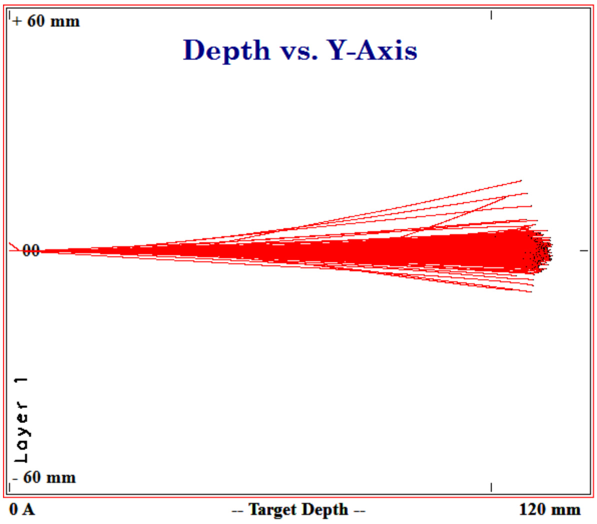

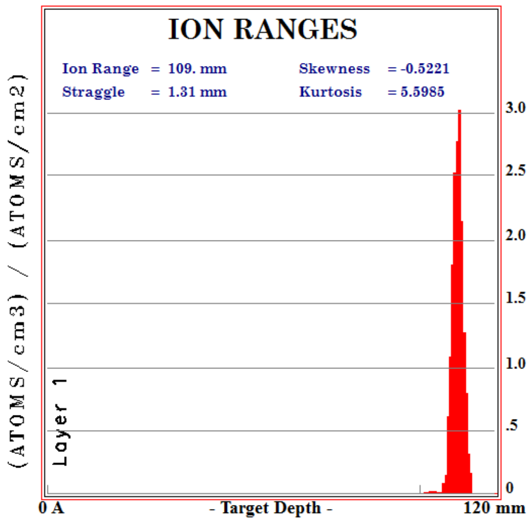

Glossary

abstraction process This is the first, often implicit, step of a finite element simulation. It aims at choosing the only relevant phenomena in the simulation in order to reduce the calculation time. For example, in order to simulate the trajectory of one planet around the sun, you may not need to take the mass of the other planets to do so since they are negligible compared to the solar mass. You could be more precise by taking into account all the other planet masses but the calculation would be much longer and not so much precise. 8

ACE Antiproton Cell Experiment.. 2

AD Antiprotons Decelerators.. 2

ALPHA Antihydrogen Laser PHysics Apparatus.. 2

ANSYS ANSYS is a finite-element Computer Aided Engineering software (CAE). It is widely spread in the industry. For more information, see `www.ansys.com/`. i, 13, 23, 25–29, 31

ASACUSA Atomic Spectroscopy And Collisions Using Slow Antiprotons.. 2

ATRAP Antihydrogen TRAP.. 2

beta function the beta function is the distance from the focus point where the beam width is twice as wide as the focus point. If the beta is high, the beam is wide and straight, it it is low, the beam is narrower and chaotic. While the emittance gives an idea of the minimal distance the beam size can be reduced to in theory, the beta function gives an idea of how wide it is at a position x (the beta function depends on where the beam is measured whereas the emittance is always the same). 5

BID Beam Intercepting Devices, for example: collimators, targets, dumps. Theses devices shares common issues such as deformation and stresses when irradiated. See figure 3.2 for those issues. 8, 9

Bragg peak Position where one particle deposits the maximum of its energy. See `http://en.wikipedia.org/wiki/Bragg_peak` for more details. ix, 18, 25

CERN Centre Europeen de Recherche Nucleaire i.e. European Center for Nuclear Research. iii, v, vii, 1–3, 20, 22, 23, 31

CES software used for rational selection of materials according to their properties. It produces 2D maps such as those found in section 5.2. See the chart 5.1. ix, 17, 19, 20, 26

CLIC The Compact Linear Collider (CLIC) Study is a site independent feasibility study aiming at the development of a realistic technology at an affordable cost for an electron-positron Linear Collider in the post-LHC era for Physics up to the multi-TeV center of mass colliding beam energy range (nominal 3 TeV). See `http://clic-study.web.cern.ch/clic-study/` for more details. 1

CLOUD Cosmics Leaving OUtdoor Droplets.. 2

CNGS Cern Neutrino to Gran Sasso. See `http://proj-cngs.web.cern.ch/proj-cngs/` for more details. 1

COMPASS COmmon Muon and Proton Apparatus for Structure and Spectroscopy.. 2

CTF3 The Clic Test Facility aims at demonstrating the feasibility of the CLIC scheme of multi-TeV electron-positron linear collider by 2010. 1

DIRAC DImeson Relativistic Complex.. 2

dispersion A particle beam is never monochromatic but has an energy spread. A physical interpretation of the dispersion is the deviation of a particle from its ideal path when it has a difference δ from the ideal momentum. 5

figure of merit See section 5.1 for definition and explanation. 17, 18, 20

FLUKA FLUKA is a fully integrated particle physics MonteCarlo simulation package. It has many applqications in high energy experimental physics and engineering, shielding, detector and telescope design, cosmic ray studies, dosimetry, medical physics and radio-biology. In the present feasibility study, is used to simulate the deposition of energy of the Linac4 beam in the materials. For more details, see `http://www.fluka.org/fluka.php`. i, 23, 25, 28, 29, 31

ISOLDE On-Line Isotope Mas separator. See `http://isolde.web.cern.ch/ISOLDE/default2.php?index=index/facilityindex.htm&main=facility/facility.php` for more details about the facility. 1, 2

LBE Diagnostic line for emittance (or energy) measurements. Before injecting the beam in the next accelerators, its "quality" (energy and energy spread) must be checked. The LBE line aims at measuring the emittance of the beam. 5

LBS Diagnostic line for energy spread measurements. Before injecting the beam in the next accelerators, its "quality" (energy and energy spread) must be checked. The LBS line aims at measuring the energy spread of the beam, which is not perfectly 160 MeV but has a spread of about $0.2MeV$. The LBS line is represented on figure 2.1. i, 1, 5, 31

LEIR Low Energy Ion Ring.. 2

LHC Large Hadron Collider.. i, 1, 2

Linac 2 Linear Accelerator of the second generation. Linear accelerator are often present between the proton source and the rings: it provides a first acceleration. The output energy of the Linac 2 is around 50 MeV. i, 1

Linac3 Linear accelerator aiming at accelerating ions before injecting them in the PSB. See figure 1.1. 2

Linac 4 Linear Accelerator of the fourth generation. Linear accelerators are present between the proton source and the rings: it provides a first acceleration. The Linac4 will replace the Linac2 in order to increase the output energy from 50 MeV to 160 MeV. This will enable the LHC to reach its highest energy. i, 1, 5, 31

predesign This term is volontarily introduced in the present feasibility study to avoid any confusion with the word design, whose definition varies from the complete description of the device to only its shape. In this study, predesign denotes the shape of the volume of interaction of the beam with the device, its phase, how it is cooled, if it has a mechanical movement or not. Considerations about how to integrate the device with the other part of the beam line, what kind of screws should be used, etc are left out. vii, ix, 9, 11–13, 20, 25–27, 31

PS Proton Synchrotron. It accelerates protons delivered from the PSB or ions from the LEIR. See `http://public.web.cern.ch/public/en/research/PS-en.html` for more details. See figure 1.1. 1, 2

PSB Proton Synchrotron Booster. See figure 1.1. 1

safety factor The safety factor is defined as the ratio of the ultimate strength a material over the maximal stress at a point. In our present study the fatigue safety factor was used and is defined by the ratio of the fatigue limit of the material at 10^7 cycles over the maximal stress in the material. The safety factor gives a value around one, it is below the material fail, if it is above it does not. 26, 27

Slit see figure 3.1. The function of a slit is to cut one part of the beam while the other goes through. The main challenge with energetic ions, such as in the present feasibility study, is to keep the aperture of the slit stable during operation. This aperture may indeed deforms during operation because the beam heats the slit, which dilates. i, viii, ix, 7–9, 33

SPS The Super Proton Synchrotron is the second largest machine in CERN accelerator facility. Measuring nearly 7 km in circumference, it takes particles from the PS and accelerates them to provide beams for the Large Hadron Collider, the COMPASS experiment and the CNGS project. See figure 1.1. 1, 2

SRIM Stopping and Range of Ions in Matter is a software that evaluate the trajectory and deposited energy of energetic ions in matter. For more information, see : `http://www.srim.org/`. 12, 14, 19, 21, 35

working temperature Temperature above which the mechanical properties of a materials decreases significantly. There does not seem to be exact definition of what is meant by "significantly", but all materials do lose their mechanical properties before they melt, be it hundreds of degrees from it or only a few degrees. The drop of the mechanical properties are then very fast. 11, 17, 25

Index

Bibliography

[1] Linac4 project. website, April 2012. URL http://linac4-project.web.cern.ch/linac4-project/.

[2] IPAC 2011, editor. Design of a Beam Dump for 3 to 100 MeV for the new H- Beam in the CERN Linac4, 2011. CERN, IPAC. C.Maglioni.

[3] A.Fasso A.Ferrari, P.R.Sala and J.Ranft. FLUKA: a Multi-Particle Transport Code. CERN, 10 2005.

[4] C.Kittel. Introduction to Solid State Physics. John Wiley and Sons, 1996.

[5] Granta Design. Granta ces selector. software. based on M.F.Ashby work.

[6] S.V. Stankus O.S. Yatsuk E.I. Zhmurikov, I.V. Savchenko and L.B. Tecchio. Measurements of the thermophysical properties of graphite composites for a neutron target converter. Nuclear Instruments and Methods in Physics Research A, pages 79–84, january 2012.

[7] J.P. Biersack J.F.Ziegler and M.D.Ziegler. Srim - the stopping and range of ions in matter, 2008. software available at: http://www.srim.org/.

[8] T.Hermanns K.Hanke. Measurement of the energy distribution of the cern linac4 160 mev h- beam close to the ps booster injection. sLHC Project Report 0033, CERN, Geneva, 23/02 2010.

[9] Cindas LLC. Cindas materials properties llc. website: https://cindasdata.com/Applications/trialAgreement.

[10] M.F.Ashby. Materials selection in mechanical design. Butterworth Heinemann, reprinted from the first edition with corrections. edition, 1997.

[11] S.Amirthatpandian C.Trautmann M.Krause, M.Tomut and W.Ensinger. Microstructural evolution of helium-implanted isotropic graphite. GSI scientific report, page 1, 2009.

[12] P.Sievers. Elastic stress waves in matter due to rapid heating by an intense high-energy particle beam. Cern internal report, CERN, Geneva, 26/06 1974.

[13] Swanson Analysis System. Ansys academic research, release 13. http://www.ansys.com.

[14] T.Hermanns. Specifications of a vertical slit for the lbs line. Functional Specification EDMS 1094603, CERN Linac4, Geneva, 02/01 2011. document at the origin of the present slit feasibility study.

[15] T.Hermanns. Measurements of energy and transverse emittance of the 160 mev linac4 h- beam before injection into the cern ps booster. Poster, 27/09 to 09/10 209. CERN accelerator school.